frontiers in Molecular Biosciences

ORIGINAL RESEARCH
published: 27 January 2022
doi: 10.3389/fmolb.2021.780192

A Transient Metabolic State in Melanoma Persister Cells Mediated by Chemotherapeutic Treatments

Prashant Karki†, *Vahideh Angardi*†, *Juan C. Mier and Mehmet A. Orman* *

Department of Chemical and Biomolecular Engineering, University of Houston, Houston, TX, United States

Persistence is a transient state that poses an important health concern in cancer therapy. The mechanisms associated with persister phenotypes are highly diverse and complex, and many aspects of persister cell physiology remain to be explored. We applied a melanoma cell line and panel of chemotherapeutic agents to show that melanoma persister cells are not necessarily preexisting dormant cells; in fact, they may be induced by cancer chemotherapeutics. Our metabolomics analysis and phenotype microarray assays further demonstrated a transient upregulation in Krebs cycle metabolism in persister cells. We also verified that targeting electron transport chain activity can significantly reduce melanoma persister levels. The reported metabolic remodeling feature seems to be a conserved characteristic of melanoma persistence, as it has been observed in various melanoma persister subpopulations derived from a diverse range of chemotherapeutics. Elucidating a global metabolic mechanism that contributes to persister survival and reversible switching will ultimately foster the development of novel cancer therapeutic strategies.

Keywords: cancer persisters, melanoma, drug-tolerance, metabolomics, chemotherapeutics, high-throughput assays

OPEN ACCESS

Edited by:
Benedicte Elena-Herrmann, INSERM U1209 Institut pour l'Avancée des Biosciences (IAB), France

Reviewed by:
Qinxi Li, Xiamen University, China
Arnaud Vigneron, INSERM U1052 Centre de Recherche en Cancerologie de Lyon, France

***Correspondence:**
Mehmet A. Orman
morman@central.uh.edu

†*These authors have contributed equally to this work*

Specialty section:
This article was submitted to Metabolomics, a section of the journal Frontiers in Molecular Biosciences

Received: *20 September 2021*
Accepted: *29 December 2021*
Published: *27 January 2022*

Citation:
Karki P, Angardi V, Mier JC and Orman MA (2022) A Transient Metabolic State in Melanoma Persister Cells Mediated by Chemotherapeutic Treatments. Front. Mol. Biosci. 8:780192. doi: 10.3389/fmolb.2021.780192

INTRODUCTION

Conventional cancer therapies target the mechanisms underlying the rapid growth of tumor cells. However, these therapies are usually inefficient for small subpopulations of persister cancer cells that are in a transient "persistence state" (Sharma et al., 2010; Ramirez et al., 2016; Hangauer et al., 2017). This phenomenon resembles bacterial persistence, which is characterized by slow growth coupled with the ability to tolerate unusually high levels of drugs and has been documented across multiple tumor cell lines and in response to a variety of therapeutic challenges (Hangauer et al., 2017). The molecular mechanisms underlying the observed tolerance of persister cells are highly complex.

Persisters are an important health concern. While persistence is defined as a transient, non-mutagenic state, it can serve as a source of drug-tolerant mutants (Ramirez et al., 2016). Persisters are also thought to underlie the proclivity of recurrent cancers to relapse (Sharma et al., 2010). Recurrence is seen in many tumor types, including skin, lung, pancreas, bladder, and breast cancers, and continues to be a major challenge in cancer therapy (Miller et al., 2019). For instance, a study performed over a period of 20 years (1994–2014) at the Beth Israel Deaconess Medical Center showed that patients with melanoma have an estimated 41.1% recurrence rate (Koolen et al., 2017). Unfortunately, melanoma is the most fatal form of skin cancer, and its incidence rate in the U.S. has tripled over the past decade (SEER Cancer Statistics, 2007). The

American *Cancer* Society estimated approximately 106,110 new cases and 7,180 deaths related to melanoma in 2021 (Jemal et al., 2018).

Conventional chemotherapy is one of the most common treatment strategies used to rapidly kill proliferating cancer cells. Unlike targeted therapeutics, chemotherapeutics may not be cancer type specific. However, according to American *Cancer* Society, chemotherapy is not often used for melanoma patients due to the reported high relapse rates (American Cancer Society, 2001). Chemotherapeutics may stimulate a persistence state in melanoma cells, which remains to be characterized. Most chemotherapeutics cause DNA damage, which induces the phosphorylation of Ataxia Telangiectasia Mutated (ATM) and Ataxia Telangiectasia and Rad3-related protein (ATR) kinases (Woods and Turchi, 2013). ATM-mediated growth arrest can be facilitated by the transcription factor p53, which activates the cyclin-dependent kinase (CDK) inhibitor p21 (He et al., 2005; Liu et al., 2019). In the absence of functional p53, ATM and ATR can still induce cell cycle arrest, as these regulators, together with Checkpoint Kinases 1 and 2 (CHK1 and CHK2), reduce CDK activity, thus resulting in cell dormancy via the inactivation of cell proliferation-related signaling pathways (Reinhardt et al., 2007). To further demonstrate whether the induction of growth arrest by chemicals is observed in skin cancer, we analyzed the Library of Integrated Network-Based Cellular Signatures (LINCS) Consortium database (Keenan et al., 2018; Niepel et al., 2019). This database, which includes more than 100,000 gene expression profiles, was generated through a data processing pipeline that captures raw data for more than 950 transcripts and infers the expression of nonmeasured transcripts for each cell line and chemical treatment condition (Keenan et al., 2018). Our bioinformatics analysis indicates that chemical treatments decrease the expression of cyclins, CDKs, and other important proteins that mediate cell division (e.g., CDK1, CCNB1, CCNB2, CCNA2, CDC25B, CDC20) in skin cancer (**Supplementary Table S1**), which is in agreement with our argument.

As we think chemotherapy can induce persistence state in melanoma cells, the metabolic alteration associated with growth arrest is inevitable during drug treatment. Metabolic reprogramming, including rapid ATP generation, increased biosynthesis of macromolecules, and maintenance of cellular redox balance under nutrient-depleted conditions and other stresses, is one of the hallmarks of cancer (Hanahan and Weinberg, 2011) and occurs to meet the essential needs of cancer cells. Aerobic glycolysis, known as the Warburg effect, is the most common feature of metabolic reprogramming observed in cancer cells. This phenomenon is characterized by the increased consumption of glucose via glycolysis and the downregulation of oxidative phosphorylation irrespective of oxygen availability and mitochondrial activity (Warburg, 1923; Warburg, 1925; Liberti and Locasale, 2016). This shift seems to be essential for supporting the large-scale biosynthetic processes that are required for active cell proliferation (Liberti and Locasale, 2016). Although aerobic glycolysis appears to occur in many rapidly dividing mammalian cells, this may not necessarily be the case in persisters, which exist in a slowly proliferating state. Metabolic alteration in persister cells potentially extends beyond glycolysis, and these cells can rely on different metabolic pathways to evade drug effects. Understanding the metabolic state of persisters will provide important insights that are likely to aid the development of novel and broadly effective cancer treatments. A recent study by Hangauer et al. (2017) presented an example of the therapeutic promise of targeting persister metabolism. Specifically, the study revealed the existence of a common survival mechanism mediated by the lipid hydroperoxidase GPX4 in persister cell populations derived from breast, melanoma, lung, and ovarian cancers. The team screened a diverse collection of compounds and found that two GPX4 inhibitors (RSL3 and ML210) were selectively lethal to persisters. In a separate study, Shen et al. (2020) revealed the existence of a metabolic mechanism, characterized by the upregulation of fatty acid oxidation, in the melanoma persister cell population mediated by BRAF and MEK inhibitors. Although many studies have shown that oxidative stress plays a critical role in persistence (Roesch et al., 2013; Viale et al., 2014; Wang L. et al., 2019), we first need to obtain a comprehensive understanding of the metabolic state of persister cells to explore their metabolism as a therapeutic target. We still need to elucidate 1) whether the metabolic alteration observed in persister cells is a hallmark of cancer persistence, 2) whether it is a transient state induced by cancer therapeutics and 3) whether it depends on drug type, concentration and treatment duration. In this study, our characterization of the metabolic mechanisms of melanoma persister cells revealed that 1) metabolic alteration associated with increased mitochondrial activity seems to be a general characteristic of melanoma persisters, 2) the observed metabolic state in persisters is transient, and 3) this metabolic state is a result of the inhibition of cell growth, which can be mediated by a wide range of chemotherapeutics.

MATERIALS AND METHODS

Cell Lines and Chemicals

The melanoma cell lines (A375 and RPMI-7951) was purchased from American Type Culture Collection (ATCC) (Manassas, VA). Unless otherwise stated, all chemicals and growth media were obtained from Fisher Scientific (Waltham, MA). A375 and RPMI-7951 cells were maintained in Dulbecco's modified Eagle's medium (DMEM) supplemented with 10% fetal bovine serum (FBS), 100 units penicillin and 100 μg streptomycin/mL at 37°C in a 5% CO_2 incubator. MitoPlates, S-1 (catalog# 14,105) containing glycolysis and Krebs cycle substrates, and I-1 (catalog # 14,104) containing ETC inhibitors were obtained from Biolog, Inc. (Hayward, CA). Saponin (catalog# 47,036), used as a cell permeabilization reagent, was purchased from Sigma Aldrich (St. Louis, MO). Phycoerythrin (PE) conjugated antibodies were purchased from BD biosciences (San Jose, CA). Stock solutions for all chemotherapeutic agents were prepared with DMSO as the solvent. Phenothiazine drugs [trifluoperazine (TFZ), thioridazine (TDZ), and fluphenazine (FPZ)] were dissolved in sterile deionized (DI) water. The cells were always cultured in DMEM at 37°C with 5% carbon dioxide (CO_2) in a

humidified incubator; they were treated with chemotherapeutics when they reached a confluency of ~40–50%.

Transcriptomics Dataset Analysis

Preliminary inspection included an analysis of the 100 most upregulated and 100 most downregulated genes in melanoma cell lines in the Broad Institute's Connectivity Map (CMAP) dataset (Keenan et al., 2018). The CMAP dataset contains information on the mRNA-level changes (in terms of transcript abundance) of a collection of 12,328 human genes after treatment with 118,050 unique perturbation agents and between cell line pairs; these expression data are collectively referred to as signatures. The data were prepared using the L1000 assay, which is used to measure the "Landmark" 978 genes that can, through computational analysis, derive sufficient information about the transcriptional state of a cell. Using this dataset, we derived the 100 most upregulated and 100 most downregulated genes by filtering the z-score data matrix to only include the A375 melanoma cell line. In the new matrix, each row represented the expression level of a gene (defined by z-score) in the melanoma cell line, and each column represented a chemical agent with which the melanoma cell line was treated. The most upregulated genes were selected by counting the number of treatments with a z-score greater than 2 for each gene ($p < 0.05$), and the top 100 genes with the highest count were reported. Likewise, the 100 most downregulated genes were selected by counting the number of treatments with a z-score less than −2 for each gene (**Supplementary Table S1**).

Persister Assays

Persister isolation was performed using a strategy published in a previous study (Shen et al., 2019). Approximately 2.5×10^6 cells were suspended in 15 ml of DMEM, plated in T-75 flasks and incubated for 24 h to obtain the desired confluency (~40–50%). Then, the medium was removed and replaced with fresh growth medium containing a chemotherapeutic agent at 10x or 100x the half maximal inhibitory concentration (IC_{50}), as listed in **Supplementary Table S2**. The control cells were treated with the solvent (i.e., DMSO) only. After 3 days of treatment, the cells were washed with 10 ml of Dulbecco's phosphate-buffered saline (DPBS) twice and detached from the flasks with 2 ml of trypsin-EDTA (0.25% trypsin and 0.9 mM EDTA) for ~1–2 min. After ~1–2 min, 5 ml of DMEM was added, and the cell suspension was transferred to a 10-ml centrifuge tube. The cell suspension was centrifuged at 800 revolutions per minute (rpm) for 5 min, and the supernatants were removed. The cell pellets were resuspended in fresh drug-free media and plated in a T-75 flask. After 24 h of incubation, dead cells floating in the culture medium were removed, and the adherent, live cells were collected for the subsequent assays described below. Of note, when the cells were treated with drugs for 9 days, the medium was changed every 3 days.

To generate kill curves, 3×10^5 cells were plated in each well of a 6-well plate with 3 ml of DMEM and incubated as described above. Similarly, the cells were treated with chemotherapeutics for 3 days and then collected to count the live cells with trypan blue staining (Louis and Siegel, 2011) using a countess II automated cell counter (catalog# A27977, Thermo Fisher Scientific). The ratio of surviving cells to untreated control cells was plotted to generate a kill curve profile.

Live/Dead Staining

After chemotherapeutic treatments, cells were collected and transferred to fresh medium in a 12-well plate. After 24 h of incubation, the medium with dead cells was removed and replaced with fresh DMEM. Live/dead staining was performed with the ReadyProbes Cell Viability Imaging Kit (Blue/Green) (catalog# R37609, Thermo Fisher Scientific) as described by the protocol provided by the vendor. Fluorescence quantification of stained cells was carried out in standard DAPI (excitation: 360 nm and emission: 460 nm) and GFP (excitation: 470 nm and emission: 525 nm) channels by EVOS M7000 florescence microscopy (catalog# AMF7000, Thermo Fisher). The NucBlue live cell reagent is cell permeant, and the NucGreen dead cell reagent is cell impermeant. Hence, dead cells emit green and blue fluorescence, while live cells only emit blue fluorescence. Live and dead cells were used as controls; dead cells were generated by treatment with 70% ethanol for 30 min.

Apoptosis

We performed apoptosis assays using the annexin-V fluorescein isothiocyanate (FITC)/propidium iodide (PI) kit (catalog# P50-929–7; Thermo Fisher Scientific). One of the early markers of apoptosis is the appearance of phosphatidylserine (PS) on the surface of the cells. PS is usually located in the membrane leaflets that face the cytosol. However, during apoptosis, PS is exposed to the outer leaflet of the cell membrane (Van Engeland et al., 1998). Annexin V binds to PS with high specificity in the presence of calcium (Wlodkowic et al., 2009). Cells treated with chemotherapeutics were resuspended in fresh medium and plated in a T-75 flask at 37°C for 24 h. After 24 h, the cells were collected and resuspended in PBS to obtain a density of 5×10^5 cells per ml. Two hundred microliters of the cell suspension was transferred to a microcentrifuge tube. The cell suspension was centrifuged at 800 rpm for 5 min. The supernatant was removed, and the pellet was resuspended in 195 μL of binding buffer. Five microliters of annexin V-FITC solution was added, and the cell suspension was incubated for 10 min at room temperature in the dark. Following incubation, the washing step was repeated to remove any excess dye. The cell pellet was resuspended in 190 μL of binding buffer and stained with 10 μL of PI for the detection of dead cells. Finally, the cell suspension was transferred to a 5-ml test tube containing PBS to obtain a final volume of 1 ml cell suspension. The sample was analyzed with a flow cytometer. The cells were excited at 488 and 561 nm to assess green (annexin V-FITC) and red (PI) fluorescence, respectively. The green fluorescence was detected with a 520 nm emission filter; the red fluorescence was detected with a 615 nm emission filter. Cells that are FITC-positive but PI-negative are in the early phase of apoptosis; cells that are both FITC-positive and PI-positive are in the late phase of apoptosis, and cells that are both FITC-negative and PI-negative are live cells. Untreated live cells, dead cells and cytarabine-treated cells were used to gate the cell subpopulations on flow cytometry

diagrams. Dead cells were generated by treatment with 70% ethanol for 30 min. Cytarabine is known to induce apoptosis (Vincelette and Yun, 2014); cells were treated with 50 μM cytarabine for 3 days before staining the cells with the dyes.

Metabolomics Study

After 3 days of gemcitabine (GEM) treatment at 10x IC_{50}, the surviving cells were collected in a 10-ml centrifuge tube, washed with 2 ml PBS by centrifugation (5 min at 800 rpm) and pooled in a microcentrifuge tube to obtain ~100 μL of cell pellet. A dry ice/ethanol bath was used to rapidly cool and freeze the cell pellet. Untreated cells were used as a control. The frozen samples were sent to Metabolon Inc. (Morrisville, NC). Metabolon's protocols were used for the sample extraction, instrument settings, and mass spectrometry (MS) conditions (see details in article (Evans et al., 2009)). Initial data analysis was performed by Metabolon. Briefly, the obtained biochemical data were normalized to the protein concentration (assessed by Bradford assay) of each respective sample. The normalized data were used to form a matrix to perform unsupervised hierarchical clustering with the Clustergram function in MATLAB. Metabolites in persisters were compared with those in control groups using ANOVA with a significance threshold of $p \leq 0.05$. A Q-value was used to estimate the false discovery rate, and low Q-values ($Q < 0.1$) indicated high confidence in the results.

MitoPlate Assay

To assess the mitochondrial function of cells, phenotype microarray plates (S-1, catalog# 14,105) were used. Mitoplate assays employ a modified version of tetrazolium dye that can be reduced intracellularly by ETC activity across the membranes of metabolically active mitochondria, resulting in the production of water-soluble formazan. The color change associated with formazan production can be detected by absorbance measurements at 590 nm (OD_{590}) and correlates with cellular ETC activities. The assay employed Biolog Mitochondrial Assay Solution (BMAS, catalog# 72,303) together with dye mixture MC (tetrazolium-based dye, catalog# 74,353) provided by Biolog, Inc. In a 50-ml sterile reservoir, 2x BMAS, MC, 960 μg/ml saponin and sterile water were gently mixed in a 6:4:1:1 ratio to obtain the assay mixture. Thirty microliters of the assay mixture was distributed to each well of the 96-well microarray and incubated at 37°C for 1 h to dissolve the preloaded substrates.

Control or chemotherapeutic-treated cells were collected in a 10-ml centrifuge tube and centrifuged at 800 rpm for 5 min. The supernatant was removed, and the cell pellet was washed with PBS twice to remove any debris. Finally, the cell pellet was resuspended in 1x BMAS to achieve a final cell density of 1×10^6 cells per ml. Thirty microliters of the cell suspension was pipetted into each well of the microarray containing the assay mixture. The final assay mixture was composed of 3×10^4 cells per well. After inoculation, the OD_{590} was measured every 10 min with a Varioskan Lux Microplate Reader (catalog# VLBL00GD0, Thermo Fisher Scientific). These data were then normalized by subtracting the absorbance readings of control (no substrate) wells.

Modified MitoPlate Assay

To verify the accuracy of the MitoPlate assay, the same procedure was repeated in a standard half-area 96-well plate with a slight modification. Similar to the MitoPlate assay described above, the assay mixture consisted of BMAS, dye and saponin. However, sterile water was replaced with a solution consisting of 96 mM Krebs cycle substrates (i.e., sodium malate, sodium fumarate or sodium succinate). 2x BMAS, MC, saponin and substrate solution were mixed at a 6:4:1:1 ratio to prepare the assay mixture, and 30 μL of the assay mixture was transferred to each well of the 96-well plate. Similarly, 30 μL of the cell suspension in 1x BMAS was added to each well of the plate containing the assay mixture so that each well contained 4 mM substrate and 3×10^4 cells. After inoculation, the OD_{590} was measured every 10 min with a microplate reader. For the control conditions, the ETC inhibitors rotenone or antimycin A were added to the assay mixtures. The final concentration of the inhibitors in the culture was 10 μM. MitoPlate data were then normalized by subtracting the absorbance readings of control (no substrate) wells.

For "no substrate" controls, the MitoPlate assays were repeated without adding Krebs cycle substrates. In this case, after mixing 2x BMAS, MC, saponin and water at 6:4:1:1 ratio, 30 μL of the assay mixture was transferred to each well of the plate. Then, 30 μL of the cell suspension in 1x BMAS was added to each well, and OD_{590} measurements were performed similarly.

Cell Growth Assay

A375 cells were stained with carboxyfluorescein succinimidyl ester (CFSE) dye using CellTrace proliferation kits (catalog# C34570, Thermo Fisher Scientific). CFSE dye can freely diffuse across the cell membrane and produce a stable fluorescent signal following an enzymatic reaction with cellular esterases (Lyons and Parish, 1994). The cells were stained with 5 μM CFSE dye following the protocol in the manual. A total of 3×10^5 stained cells were seeded in each well of a 6-well plate and incubated for 24 h. After 24 h, the medium was removed and replaced with fresh DMEM with chemotherapeutic agents at the indicated concentrations. The cells were treated for 6 days, and the growth medium was changed every 3 days. Every 24 h, cells were detached from the wells with trypsin, collected and resuspended in 1 ml PBS for analysis with a flow cytometer. The cells were excited at 488 nm, and green fluorescence was detected with a 520-nm emission filter. The fluorescence half-life for all conditions was calculated using the decay equation below:

$$F = F_o 2^{\frac{-(t-t_o)}{t_d}}$$

where F_o is the mean fluorescence intensity for cells at time t_o; t_d is the half-life time; and F is the mean fluorescence intensity for cells at time t. In this study, t_o was chosen as day 0. The half-life time was calculated with SOLVER in Excel by minimizing the sum of normalized mean square errors (NMSE) between experimental and predicted model data.

Microscopy Analysis for Cell Growth

Cells were stained with 5 μM CFSE dye following the protocol provided in the CellTrace kit. A total of 3×10^5 cells were then

seeded in each well of a 6-well plate and incubated for 24 h. After 24 h, the medium was removed from each well and replaced with medium including a chemotherapeutic agent. After 3 days of incubation, cells were washed with 3 ml DPBS, detached with 200 μL of trypsin, resuspended in 1 ml medium, transferred to a 1.5-ml microcentrifuge tube and centrifuged at 800 rpm for 5 min. The supernatant was removed, and the cell pellet was resuspended in 1 ml fresh drug-free growth medium and transferred to each well of a 6-well plate. After 24 h of incubation, the growth medium was replaced with 1 ml DPBS. The cells were then analyzed under an EVOS M7000 fluorescence microscope (excitation: 470 nm and emission: 525 nm).

ALDEFLUOR Assay

An ALDEFLUOR assay kit (catalog# NC9610309, Thermo Fisher Scientific) was used to measure the cellular aldehyde dehydrogenase (ALDH) activity. A total of 3×10^5 cells were plated in each well of a 6-well plate with 3 ml of DMEM and incubated for 24 h. After 24 h, the growth medium was removed and replaced with fresh growth medium containing a chemotherapeutic agent. Every 24 h, the cells were washed with 3 ml DPBS, detached with 200 μL trypsin, resuspended in 1 ml growth medium and transferred to a microcentrifuge tube. The cell suspension was centrifuged at 800 rpm for 5 min, and the supernatant was removed. This washing procedure was repeated with DPBS to remove all the residuals. Finally, the cell pellet was resuspended in 1 ml of ALDEFLUOR assay buffer. Five microliters of the activated ALDEFLUOR reagent was added to the cell suspension and mixed. After mixing, 500 μL of the cell suspension was immediately transferred to another microcentrifuge tube containing 5 μL of diethylamino-benzaldehyde (DEAB), which was used as a negative control, as DEAB inhibits ALDH activity. The samples were then incubated at 37°C for 45 min. After incubation, the cell suspension was centrifuged at 800 rpm for 5 min, and the supernatant was removed. The cell pellet was resuspended in 500 μL of ice-cold ALDEFLUOR assay buffer and transferred to a 5-ml test tube. Each sample was stained with 1.5 μM PI, incubated for 15 min at room temperature and analyzed by flow cytometry. The cells were excited at 488 and 561 nm for green and red fluorescence, respectively. The green fluorescence was detected with a 520-nm emission filter; the red fluorescence was detected with a 615-nm emission filter.

Measuring CD271, CD44 and CD34 Biomarkers

Approximately, 2.5×10^6 cells were seeded in a T-75 flask containing 15 ml of DMEM and incubated for 24 h. After 24 h, cells were either treated with a chemotherapeutic agent or left untreated. At indicated time points, cells were detached, collected in a 15 ml centrifuge tube, centrifuged at 800 rpm for 5 min and the supernatant was discarded. The cells were then washed with 5 ml of DPBS. Finally, 1×10^6 cells were resuspended in 100 μL of cell stain buffer (catalog# 554,657) in a microcentrifuge tube. Then, 20 μL of a Phycoerythrin (PE) conjugated antibody [CD271 (catalog# 557,196), CD44 (catalog# 555,479), or CD34 (555,822); BD Biosciences, San Jose, CA] or its respective IgG control was added and the cell suspension was incubated at room temperature for 30 min. After incubation, the cells were centrifuged at 800 rpm for 5 min and the supernatant was discarded. The cell pellet was resuspended in 500 μL of cell stain buffer, stained with 0.25 μM of SYTOX green and incubated for 15 min at room temperature. The cells were then transferred to a 5 ml test tube and analyzed with a flow cytometer. The cells were excited at 488 and 561 nm for green and red fluorescence, respectively. The green fluorescence was detected with a 520-nm emission filter; the red fluorescence was detected with a 586-nm emission filter.

Inhibitor Screening

Approximately 1×10^4 cells were suspended in 150 μL of DMEM, plated in each well of a 96-well plate and incubated for 24 h. Then, the medium was removed and replaced with 150 μL of DMEM containing GEM (20 nM) and/or the ETC inhibitors obtained from the Biolog I-1 plate (catalog # 14,104). Of note, the ETC inhibitors are in their solid forms in the I-1 plate; therefore, 150 μL of DMEM with or without GEM was added to each well of the I-1 plate in advance. After 2 h of incubation, the media were transferred from the I-1 plate to the 96-well plate containing the cells mentioned above. After 3 days of treatment, the medium was removed, and the cells were washed with 100 μL of DPBS twice. Then, 150 μL of drug and inhibitor-free medium was transferred to each well of the 96-well plate. After incubating the cells for 24 h, the growth medium was removed and replaced with 100 μL of fresh medium. Finally, 10 μL of 3-(4,5-dimethylthiazol-2-yl)-2,5-diphenyltetrazolium bromide (MTT, catalog # 97,062–376, VWR) (5 mg/ml) was added to each well to measure the cell viability, and the cells were incubated at 37°C for 3 h. At 3 h, the medium was removed and replaced with 100 μL of MTT solubilization buffer (Riss et al., 2004). After 20 min of incubation at 37°C, the absorbance at 570 nm (OD_{570}) was measured with a microplate reader.

Validation of the Inhibitor Screening Assay Results

A total of 3×10^5 cells were plated in each well of a 6-well plate with 3 ml of DMEM and incubated for 24 h as described above. The cells were cotreated with GEM and/or phenothiazine for 3 days. After 3 days, the surviving cells were washed with 2 ml DPBS, detached with 200 μL of trypsin for 1–2 min, resuspended in fresh drug-free DMEM and incubated for 24 h. After 24 h, the cells were collected as described above, transferred to a microcentrifuge tube in PBS, and enumerated with trypan blue solution (0.4%) and the automated cell counter. If the surviving cell levels were under the limit of detection, we used a flow cytometer. To do this, the cell suspension was centrifuged at 800 rpm for 5 min, and the supernatant was removed. The cell pellet was resuspended in 500 μL of 0.85% sodium chloride (NaCl) solution. Then, the cells were stained with 0.25 μM SYTOX green (catalog # S7020, Thermo Fisher Scientific) and SYTO60 red (catalog # S11342, Thermo Fisher Scientific) and then incubated at 37°C for 15 min. SYTOX green is cell

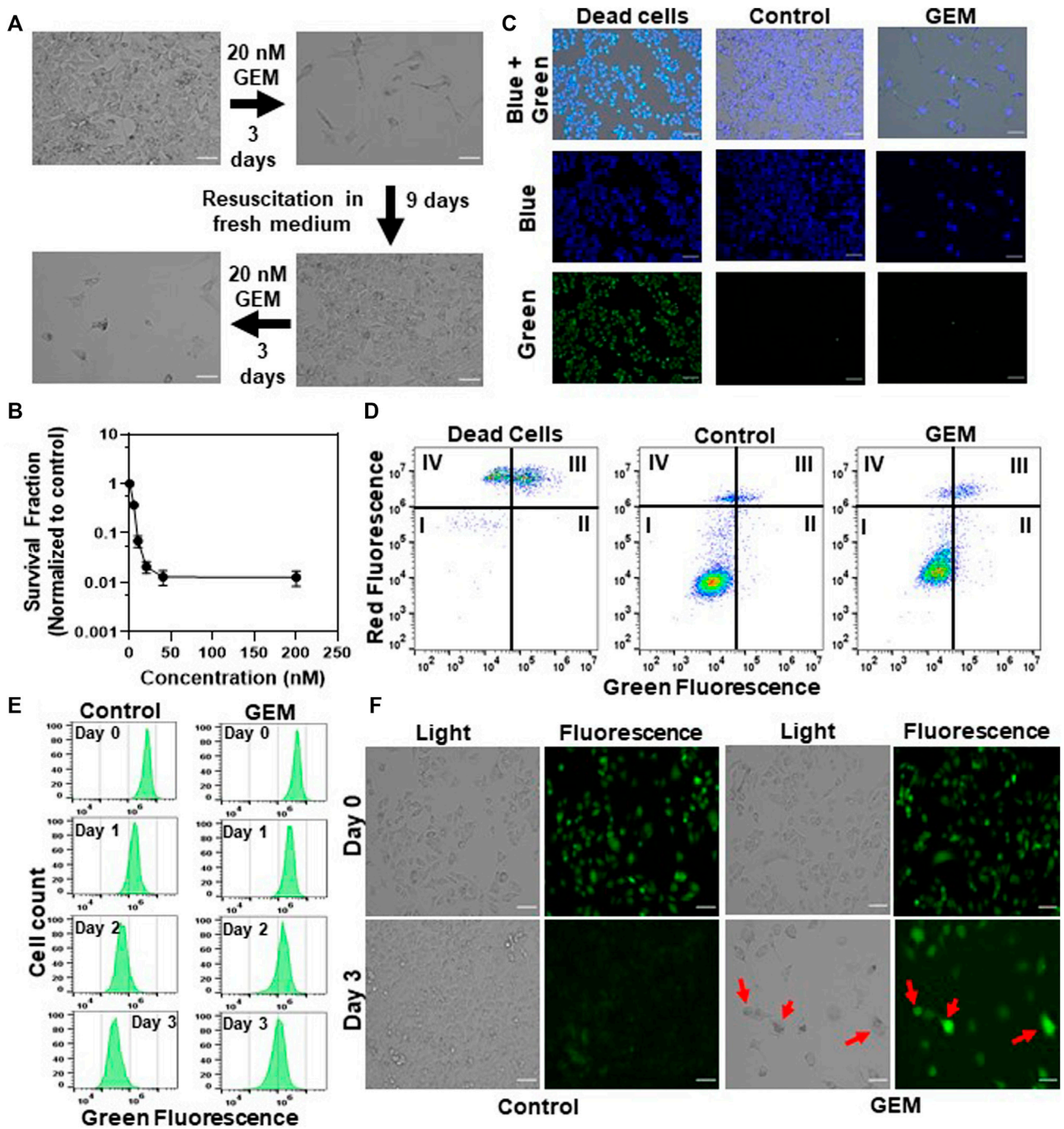

FIGURE 1 | Isolating drug-tolerant persister cells: **(A)** A375 melanoma cells were treated with GEM ($10xIC_{50}$ = 20 nM, see **Supplementary Table S2**) for 3 days. After the treatment, cells were allowed to recover in fresh, drug-free growth medium and then treated with GEM after recovery to demonstrate the sensitivity of the daughter cells to GEM. Scale bar: 100 μm. **(B)** A375 cells were treated with GEM at the indicated concentrations for 3 days. The surviving cells after the treatment were collected and transferred to fresh medium without GEM. The following day, cell viability was assessed by trypan blue staining (see *Materials and Methods*). Survival fractions were calculated by normalizing the surviving cell numbers to those in the untreated control groups. The number of biological replicates (*N*) = 4. **(C)** The cells surviving after GEM treatment were collected and transferred to fresh medium without GEM. The following day, cells were stained with ReadyProbes Cell Viability Imaging dyes to assess live and dead cells. The blue probe stains the nuclei of all cells, and the green probe only stains the nuclei of cells with compromised membranes. Dead cells were generated by treating the cells with 70% ethanol for 30 min. "Control" represents the live cells that did not receive GEM treatment. Scale bar: 100 μm. **(D)** Cells after GEM treatment were collected and transferred to fresh medium without GEM. The following day, cells were stained with FITC-annexin-V conjugate and PI to detect apoptotic cells. The quadrants of this graph represent (I) live (FITC-/PI-), (II) early apoptotic (FITC+/PI-), (III) late apoptotic (FITC+/PI+) and (IV) dead (FITC-/PI+) cells. **(E, F)** Melanoma cells prestained with CFSE dye were treated with GEM or left untreated (control), and their fluorescence intensity was monitored at the indicated time points with flow cytometry **(E)** or florescence microscopy **(F)**. *N* = 4. Scale bar: 100 μm.

impermeant and only stains dead cells. SYTO60 is cell permeant and can diffuse through the cell membrane. After 15 min, the cell suspension was centrifuged at 800 rpm for 5 min, and the supernatant was removed. Finally, the cell pellet was resuspended in 500 µL of 0.85% NaCl solution and transferred to a 5-ml test tube for flow cytometry analysis. The cells were excited at 488 nm for green fluorescence and 561 nm for red fluorescence. The green fluorescence was detected with a 520-nm emission filter; the red fluorescence was detected with a 615-nm emission filter.

Statistical Analysis

GraphPad Prism 8.3.0 was used for linear regression analysis, and the slopes of untreated and treated groups were compared with F statistics. Pairwise comparisons were performed using unequal variance t-tests or ANOVA. For statistical significance analysis, the threshold value of p was set as $^{*\text{ or }\#}p < 0.05$, $^{**}p < 0.01$, $^{***}p < 0.001$, and $^{****}p < 0.0001$. A minimum of three independent biological replicates (unless otherwise stated) were assessed for all experiments. In all figures, data corresponding to each time point represent the mean value ±standard error.

RESULTS

Gemcitabine Persistence Is a Slow-Growing Cell State

Persister cells are defined as a small subpopulation of phenotypic variants that are transiently tolerant to drugs. Once the drug is removed and the persisters are re-cultured in fresh, drug free medium, they form cell populations that exhibit drug sensitivity identical to the original culture, which distinguishes them from resistant mutants (Hangauer et al., 2017). In this study, persister subpopulations were derived from gemcitabine (GEM)-treated A375 melanoma cell cultures (**Figure 1A**). The A375 cell line has BRAF V600E mutations, leading to excessive cellular proliferation and differentiation and increased cell survival (Davies et al., 2002). GEM is a nucleoside that is an analog of deoxycytidine (Noble and Goa, 1997) which inhibits DNA replication by incorporating itself at the end of the elongating DNA strand. As persister cells have the ability to tolerate high concentrations of drugs, we treated A375 cells with GEM for 3 days to generate a concentration vs. survival ratio profile (**Figure 1B**); the results showed that the cell survival ratio did not change significantly at concentrations higher than $10xIC_{50}$ (20 nM, see **Supplementary Table S2**) (Yang et al., 2013; Iorio et al., 2016). After 3 days of GEM treatment, we gently detached the cells from the flasks, resuspended them in fresh, drug-free growth medium, and incubated them for 24 h to remove dead/late apoptotic cells and collect the persister cells. As shown in the microscope images from the live/dead staining assay (**Figure 1C**), nearly all persister cells were viable. Furthermore, an annexin-V fluorescein isothiocyanate (FITC)/propidium iodide (PI) assay (Wlodkowic et al., 2009) was performed to detect apoptotic cells. The data showed that the apoptosis levels in both the parental and surviving persister cell populations were nonsignificant (**Figure 1D**). Unlike drug-resistant mutants, the progenies of persisters are susceptible to cancer drugs; this phenomenon has been demonstrated in many other studies (Sharma et al., 2010; Hangauer et al., 2017; Shen et al., 2020). Therefore, cells surviving GEM treatment were transferred to fresh medium, regrown, and retreated with GEM to verify the transient state of melanoma persister cells (**Figure 1A**).

To measure the growth rate of GEM persister cells, we performed a cell proliferation study using carboxyfluorescein succinimidyl ester (CFSE) dye. For this assay, the cells prestained with CFSE were treated with GEM or left untreated (control), and the cell proliferation rates of these groups were measured by monitoring the fluorescence dilution rate over time with a flow cytometer. Our results revealed ongoing cell division in the control groups, as evidenced by a reduction in the fluorescent signals, whereas the fluorescent signal was maintained in the treatment groups largely due to a lack of cell proliferation (**Figure 1E** and **Supplementary Figure S1**). The mean fluorescence intensity for the first 3 days for each group was integrated into the fluorescence decay equation to calculate the half-life of the fluorescent signal, further showing that cells treated with GEM grew significantly slower than untreated control cells (**Supplementary Figure S1**). Our microscope images further showed that the surviving cell populations seemed to be heterogeneous (**Supplementary Figure S2**). We noticed that GEM treated cells underwent morphological changes; typically, the cells became elongated or spherical while retaining their fluorescence levels (*e.g.*, cells highlighted with arrows in **Figure 1F**).

Melanoma cells can undergo reversible phenotypic transitions in response to drug treatments, which may result in stem cell like characteristics (Keener, 2016; Rambow et al., 2019). Since high aldehyde dehydrogenase (ALDH) activity and increased expression of stem cell biomarkers, CD271, CD44 and CD34, were shown to be associated with the phenotypic plasticity of melanoma cells (Held et al., 2010; Luo et al., 2012; Paulis et al., 2015; Restivo et al., 2017), we performed the ALDEFLUOR assay and flow cytometry analysis to measure these biomarkers in GEM treated cells. Although GEM treatment slightly induced the CD271 expression in the cells, we did not observe a consistent trend in the expression levels of other stem cell biomarkers (CD44 and CD34) and found no significant increase in ALDH activity in GEM persisters compared to untreated control cells (**Supplementary Figures S3A–D, S4**). Altogether, our data indicate that persister populations studied here are slow-growing cells that are potentially induced by chemotherapeutic treatment. These cells exhibit heterogenous morphology without having a drastic increase in the expression levels of known stem cell biomarkers.

Persister Cells Have An Altered Metabolic State

Tumor cells undergo metabolic alteration to fulfill the energy requirement, sustain the high rate of cell proliferation, avoid the action of therapeutics and improve the overall survivability of the tumor cells (Sciacovelli et al., 2014). As persistence is a transient state, we expected that persister cells would undergo metabolic

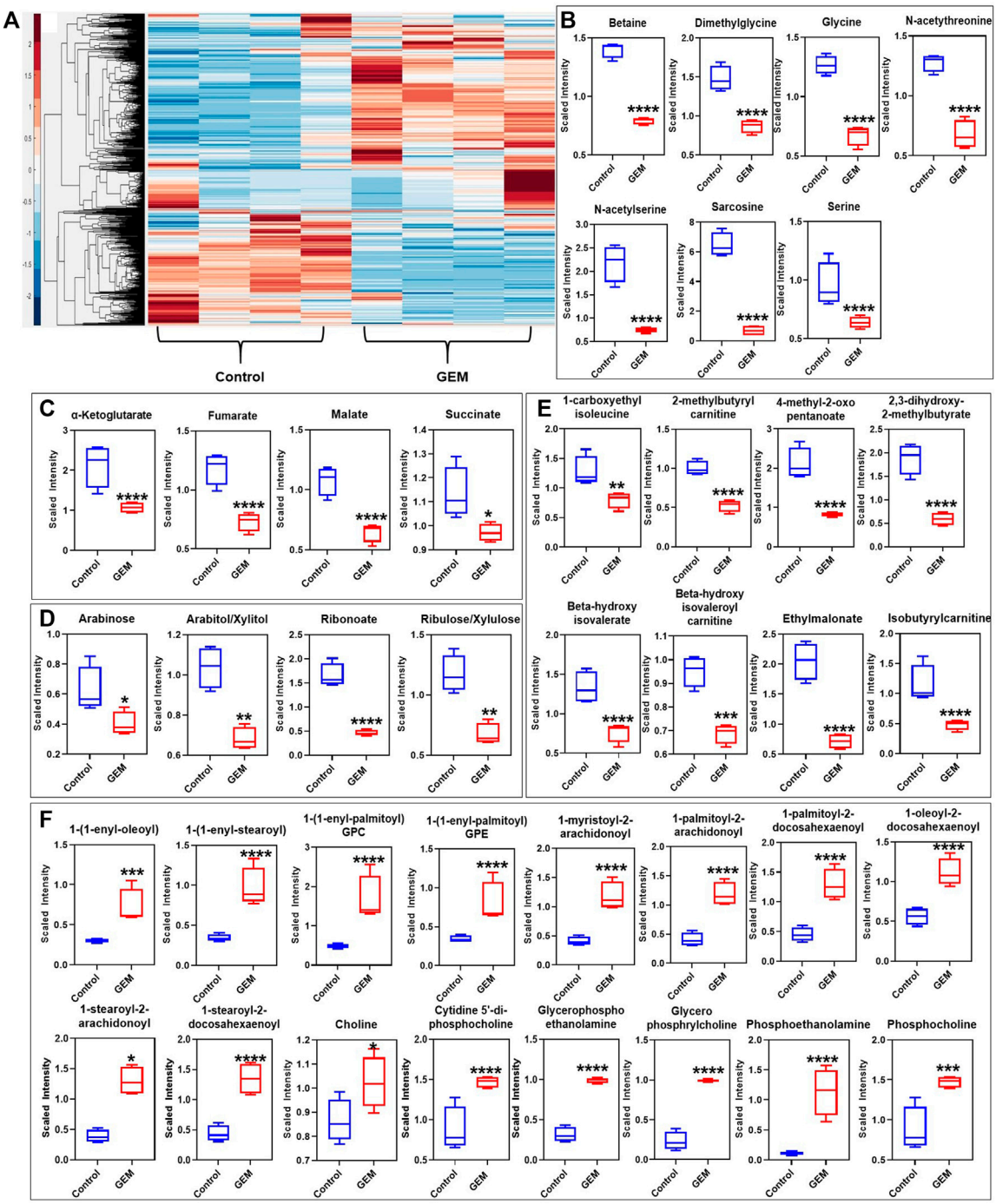

FIGURE 2 | Metabolic alterations in GEM persisters: **(A)** GEM-treated and untreated A375 cells were collected for MS analysis to measure their metabolite contents. Unsupervised clustering of the metabolomics data was performed with the Clustergram function in MATLAB. The generated heat maps show metabolite clusters that are upregulated (red) or downregulated (blue) in the treated group compared to the untreated control group. Each column represents a biological replicate; each row represents a metabolite. $N = 4$. **(B–F)** Box plots show the metabolites from the one-carbon metabolism pathway **(B)**, the Krebs cycle **(C)**, the PPP **(D)**, the BCAA metabolism pathways **(E)**, and the lipid metabolism pathway **(F)** that are significantly altered in GEM persisters compared to control cells. Statistical significance was assessed with ANOVA (*$p < 0.05$, **$p < 0.01$, ***$p < 0.001$, and ****$p < 0.0001$). $N = 4$.

alterations due to their slow or nonproliferating cell state. To identify such metabolic mechanisms, we conducted untargeted metabolomics analysis of GEM-treated cells and untreated control cells. Persisters were generated by treating the cells with 10xIC_{50} of GEM, and untreated cells were generated by culturing the cells in drug-free growth media. In our study, we

measured 689 different metabolites that are part of the superpathways involving the following factors: amino acids, peptides, carbohydrates, energy, lipids, nucleotides, cofactors/vitamin and xenobiotics (**Supplementary Table S3**). Pathway enrichment analysis showed that the relative levels of 342 metabolites were significantly altered in the persister subpopulation compared to the control group (**Supplementary Table S3**). Unsupervised hierarchical clustering of the metabolic data of four independent biological replicates of untreated or GEM-treated samples reveals a distinct metabolic alteration taking place in persister cells (**Figure 2A**). While the relative levels of metabolites associated with dipeptides, phospholipids, sphingosines, the urea cycle, gamma-glutamyl amino acid, ceramides, polyamines, tryptophan, sterols, endocannabinoid, phosphatidylcholines (PC), lysophospholipids and sphingomyelins were upregulated, those associated with glycine, serine, threonine, pentose sugars, vitamin B6, glutamate, the Krebs cycle and branched-chain amino acids (BCAAs) were significantly downregulated in persister cells compared to those in control cells (**Figures 2A–F** and **Supplementary Table S3**).

Although our metabolomic analysis indicates that the levels of phospholipids (particularly PCs, phosphatidylserine, phosphatidylethanolamine, phosphatidylglycerol, phosphatidylinositol and phosphatidylinositol-phosphates), and sphingolipids with their associated structural elements (ceramide and sphingosine) were considerably upregulated (**Figure 2F**), those involved in one-carbon metabolism (e.g., glycine, serine, and methionine) were distinctively downregulated in GEM-treated cells compared to untreated control cells (**Figure 2B**). Alteration of the lipid metabolism of cancer cells compared to that of nonmalignant cells is a well-studied phenomenon (Islam and Manna, 2019). This metabolic reprogramming has been shown to be highly dependent on the cancer type and stage. Phospholipids are predominant components of the cell membrane that can play an important role in persistence by modulating the expression and activity of multidrug resistance pumps (Kopecka et al., 2020). Sphingolipids are another family of membrane lipids known to play a role in the regulation of cell proliferation, apoptosis, migration and inflammation (Ponnusamy et al., 2010). One-carbon metabolism, as an indicator of the cell nutrient status, functions in the biosynthesis of nucleotides as well as the maintenance of the redox and methylation states required to support the high rate of proliferation in cancer cells (Newman and Maddocks, 2017).

Cancer cells overexpress amino acid-degrading enzymes to increase their energy production and to provide metabolites for their anabolic processes. BCAAs (such as leucine, isoleucine and valines) are a class of amino acids and their levels were significantly downregulated in GEM-treated cells (**Figure 2E**). BCAAs are expected to be upregulated in normal cancer cells, as they can be used for various processes such as protein synthesis and energy production (Shimomura and Kitaura, 2018). Of the carbohydrate family, the pentose phosphate pathway (PPP) metabolite levels were significantly downregulated in GEM-treated cells (**Figure 2D**). Similar to one-carbon metabolism, the PPP was shown to be important for tumor cells in terms of nicotinamide adenine dinucleotide phosphate (NADPH) production, which is essential for fatty acid synthesis and reactive oxygen species detoxification (Stincone et al., 2015). The PPP is tightly interconnected with glycolysis and the Krebs cycle, as they share a number of intermediates, including glucose-6-phosphate (G-6-P), pyruvate and acetyl-CoA. The Krebs cycle is also closely linked to BCAA metabolism, as alpha-ketoglutarate is essential for BCAA metabolism. Our untargeted metabolomics analysis showed that, similar to BCAA and PPP metabolism, the Krebs cycle was significantly altered in GEM-treated cells, as its intermediates (e.g., alpha-ketoglutarate, fumarate, malate, and oxaloacetate) were significantly less abundant in melanoma persisters than in the untreated bulk cell population; however, we did not observe a significant change in glycolysis intermediates, except for pyruvate, in either group (**Figure 2C** and **Supplementary Table S3**). Although our MS analysis shows a metabolic alteration in energy metabolism in persister cells, MS does not directly measure intracellular reaction rates (e.g., mitochondrial activity); such measurements are necessary to link the abundance of these metabolites to their turnover rates.

Persister Cells Have Increased Mitochondrial Activity

Cancer cells are known to use aerobic glycolysis to generate substrates for the anabolic processes needed to support cell proliferation (Warburg, 1925; Liberti and Locasale, 2016). We think that, due to their nonproliferating cell state (Sharma et al., 2010; Hangauer et al., 2017), persisters may have increased mitochondrial metabolism. This metabolic alteration may explain the low levels of Krebs cycle intermediates observed in persisters, as the depletion of these substrates is potentially due to faster consumption of these compounds in persisters. To verify this, we measured the mitochondrial activity of the persister cells using MitoPlates (Biolog Inc., Hayward, CA).

For this assay, 30 different substrates associated with glycolysis and the Krebs cycle were screened in a 96-well format. A kinetic graph was generated to illustrate the consumption of each substrate by measuring the color intensity of a modified tetrazolium dye present in each well. This color change correlates with cellular ETC activities. The obtained data were then clustered (unsupervised) to generate a heat map (**Figure 3A**) for all the substrates being studied. Of all the substrates that were tested, persister cells had a higher rate of consumption of Krebs cycle metabolites (specifically, the consumption rates of malate, fumarate and succinate) than untreated cells. Mitoplate screening is a high-throughput assay with limited control over the concentrations of substrates in microarrays. As the concentrations of the substrates were not disclosed, to verify the observed results, these assays were repeated in a generic 96-well plate where the metabolites (i.e., malate, fumarate and succinate) were added manually to achieve a final concentration of 4 mM. The data generated from these modified assays were in agreement with our MitoPlate data (**Figures 3B–D**). To further verify the accuracy of the assays, control experiments, in which ETC complexes were inhibited

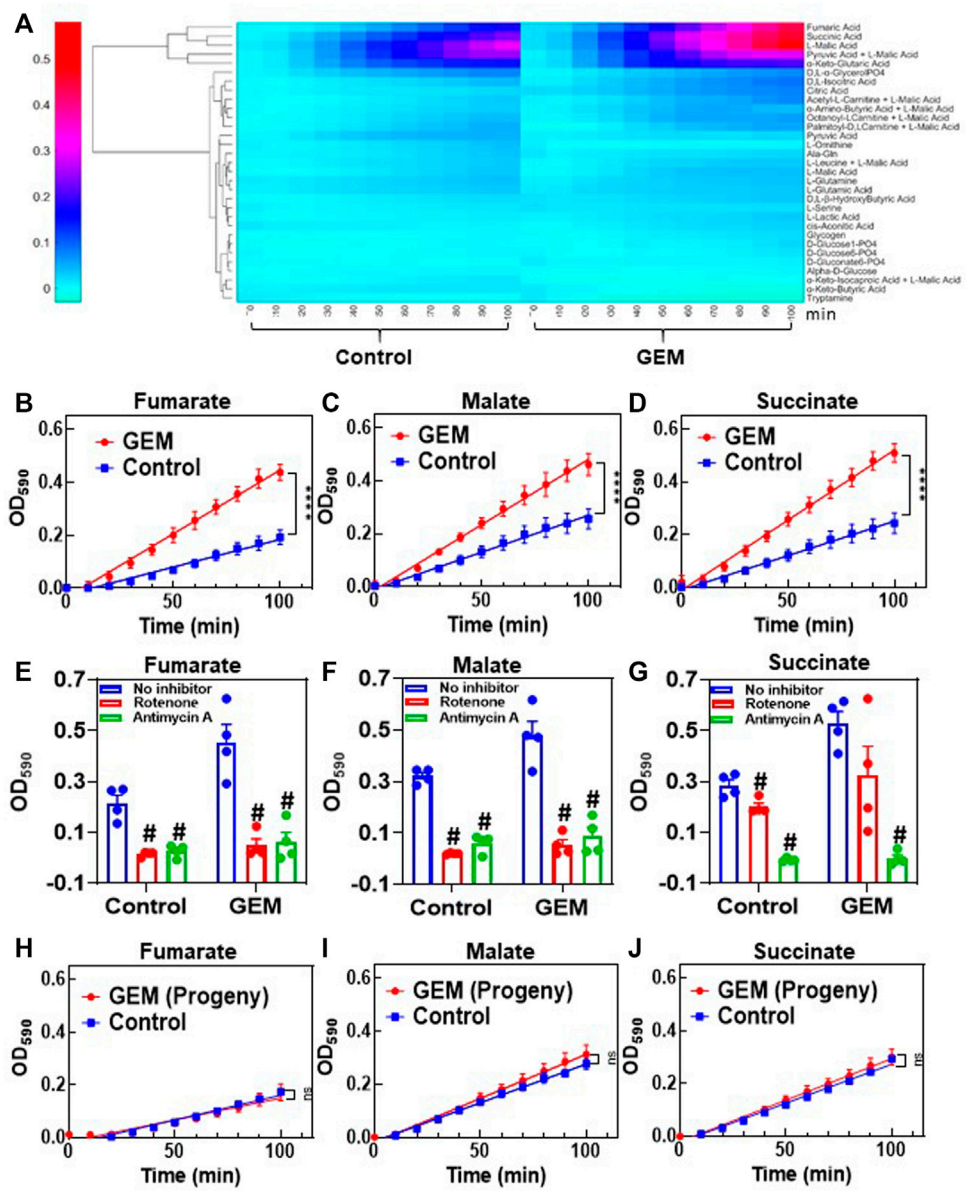

FIGURE 3 | Transient upregulation of Krebs cycle activity in GEM persisters: **(A)** Phenotype microarrays were used to assess the mitochondrial activities of GEM persister cells; 3×10^4 persister or untreated (control) A375 cells were transferred to each well of a phenotype microarray that also included a substrate and tetrazolium-based dye. The consumption rates of substrates were monitored by measuring the OD_{590} at the indicated time points (for 100 min total). Unsupervised clustering of absorbance data was performed using MATLAB. $N = 4$. **(B–D)** The consumption rates for the selected substrates (4 mM) (fumarate, malate and succinate) were measured with the modified MitoPlate assay (see Materials and Methods). Linear regression analysis was performed using F statistics with GraphPad Prism (****$p < 0.0001$). $N = 4$. **(E–G)** Bar graphs represent the OD_{590} data of the modified MitoPlate assays for fumarate, malate and succinate and indicate their consumption rates at 100 min in the presence of rotenone (10 μM) or antimycin A (10 μM). $N = 4$. Statistical significance was assessed by performing pair-wise *t*-test. # represents a significant difference between the inhibitor (rotenone or antimycin A) and "no inhibitor" groups ($p < 0.05$). **(H–J)** Persister cells were transferred to fresh medium without GEM to stimulate resuscitation. After the third passage, the daughter cells were collected, and their consumption rates for fumarate, malate and succinate were measured with the modified MitoPlate assay. Untreated parental cells were used as a control. $N = 4$; ns: the slopes are not significantly different.

with rotenone and antimycin A, were conducted. Rotenone is a complex I inhibitor, and antimycin A inhibits complex III of the ETC (Li et al., 2003; Huang et al., 2005). Therefore, the substrates capable of producing only NADH (i.e., malate and fumarate) and the substrates producing both NADH and $FADH_2$ (i.e., malate, fumarate and succinate) should not give any absorbance reading in the presence of rotenone and antimycin A, respectively, in modified MitoPlate assays. The data generated support our argument and validate the efficacy of the assay (**Figures 3E–G**). Of note, MitoPlate data reported here were normalized to "no substrate" controls in which the assays were performed without adding any exogenous Krebs cycle substrates. Critically,

these "no substrate" data still show that the basal level of persister cell ETC activity is higher than that of the untreated cells (**Supplementary Figure S5**).

Finally, as persistence is a temporary state, the observed metabolic alteration should also be transient. Cells that survived GEM treatment were collected and regrown in fresh growth medium. After 9 days of resuscitation, the cells resumed their growth cycle and started to proliferate (**Figure 1A**). The progenies of the resuscitated cells after the 3rd passage were collected to assess their mitochondrial activity. As expected, the consumption rates of malate, fumarate and succinate in persister progenies were similar to those of untreated control groups (**Figures 3H–J**).

The Observed Metabolic Alteration Is Independent of Gemcitabine Concentration and Treatment Time

The treatment duration and chemotherapeutic concentration can play a significant role in persister cell metabolism. To assess the effect of the treatment period, A375 cells were treated with GEM ($10xIC_{50}$) for 9 days, and the surviving cells were collected for MitoPlate assays, which showed that the consumption rates of Krebs cycle substrates were still higher in GEM-treated cells than in untreated control cells (**Supplementary Figure S6A**). However, interestingly, the control cells cultured for 9 days had higher consumption rates of Krebs cycle substrates than the control cells cultured for 3 days (control groups in **Supplementary Figures S6A,B**). This observation might be due to the cell-cycle arrest induced by overpopulation in 9-days cell cultures, which is consistent with our central argument. To assess the effects of drug concentrations on persister metabolism, we isolated persisters by treating the cells with $100xIC_{50}$ GEM for 3 days (**Supplementary Figures S6C,D**). Similar to the $10xIC_{50}$ treatment results, the surviving cells exhibited higher rates of consumption for Krebs cycle substrates than untreated cells (**Supplementary Figures S6B,G–I**). Persister cells obtained by $100xIC_{50}$ GEM treatment were resuspended for a second round of cell survival and MitoPlate assays, showing that the progenies of persister cells were sensitive to GEM, and the observed metabolic alteration was reversible (**Supplementary Figures S6J–L**). Persister cells obtained from $100xIC_{50}$ GEM treatment were also viable, grew slowly, and exhibited morphological heterogeneity without a consistent trend in the expression of stem cell biomarkers (**Supplementary Figures S6C–F**), in agreement with the data generated from $10xIC_{50}$ treatments. Interestingly, the cells surviving $100xIC_{50}$ GEM treatment required ~32 days to resuscitate. This was significantly longer than the resuscitation period of the $10xIC_{50}$ treatment group (~9 days), indicating that the resuscitation period is concentration dependent, although increasing the GEM concentration does not affect metabolic alteration.

Chemotherapeutic-Induced Metabolic Alteration Is Conserved in Melanoma Persisters

Next, we sought to test whether the observed results were also valid for the other chemotherapeutic agents listed in **Supplementary Table S2**. Cytarabine (CYT) is an antimetabolite similar to GEM; camptothecin (CAM), doxorubicin (DOX) and etoposide (ETO) inhibit topoisomerase; cisplatin (CIS) and temozolomide (TEM) are an alkylating agent; vinorelbine (VIN) and paclitaxel (PAC) impair the formation of spindle fibers; and mitomycin-c (MIT) induces cross-linking of DNA (Wishart et al., 2006). Cells were treated with these therapeutic agents at $10xIC_{50}$ doses (**Supplementary Table S2**), except TEM, which was applied at $5xIC_{50}$, as the $10xIC_{50}$ dose required a high dimethyl sulfoxide (DMSO) solvent content (>1%). Live/dead staining was performed for all treatments to ensure high persister cell viability (**Supplementary Figure S7**). The mitochondrial activity for each treatment was assessed using modified MitoPlate assays, which demonstrated that the chemotherapeutic agents generally increased the consumption rates of Krebs cycle substrates in melanoma cells (**Figure 4A**). Furthermore, we performed flow cytometer staining assays for stem cell biomarkers for all treatment groups (**Supplementary Figures S8, S9**). Similar to the results obtained from the GEM treatment, most treatments did not significantly alter cellular stem cell biomarker levels. However, TEM- and MIT-treated cells showed significantly lower ALDH activity than control cells, further supporting that chemotherapeutic persistence may not be directly linked to stem cell phenotypes. Our flow cytometry- and microscopy-based cell proliferation assays further showed that cells from all treatment groups had undergone a state of negligible growth, indicating that chemotherapeutic-induced growth arrest is conserved in melanoma cells (**Figure 4B**, **Supplementary Figures S1, S10**). Our microscopy images showed that when compared to the untreated control cells, treated cells had altered morphology with high fluorescence intensity due to the induction of growth arrest (**Figure 4B** vs. control group in **Figure 1F**). Overall, the upregulation of Krebs cycle activity is conserved in melanoma persister populations derived from various chemotherapeutic treatments, despite the diverse morphological changes observed in these persister populations (**Figure 4B** and **Supplementary Figure S7**).

Phenothiazine Drugs can Compromise Persister Survival

We screened a microarray plate (I-1 plates from Biolog, Inc.) with known mitochondrial inhibitors to test the effects of these inhibitors on persister cell viability, as some of these inhibitors, such as gossypol, valinomycin and celastrol, are known to stimulate the production of apoptotic reactive oxygen species (Chen et al., 2011; Lofrumento et al., 2011; Arinbasarova et al., 2012). The chemical library had four concentrations of each inhibitor, but these concentrations were not disclosed by the company (Biolog, Inc.). As we wanted to identify a chemical compound that is selectively and effectively lethal to GEM persisters, we focused on the wells with the lowest inhibitor concentrations (**Figures 5A,B**). Our initial screening is based on a tetrazolium-based calorimetric assay that measures cell metabolic activity (see *Methods*). Our data revealed that trifluoperazine (TFZ) might be a potential chemotherapeutic

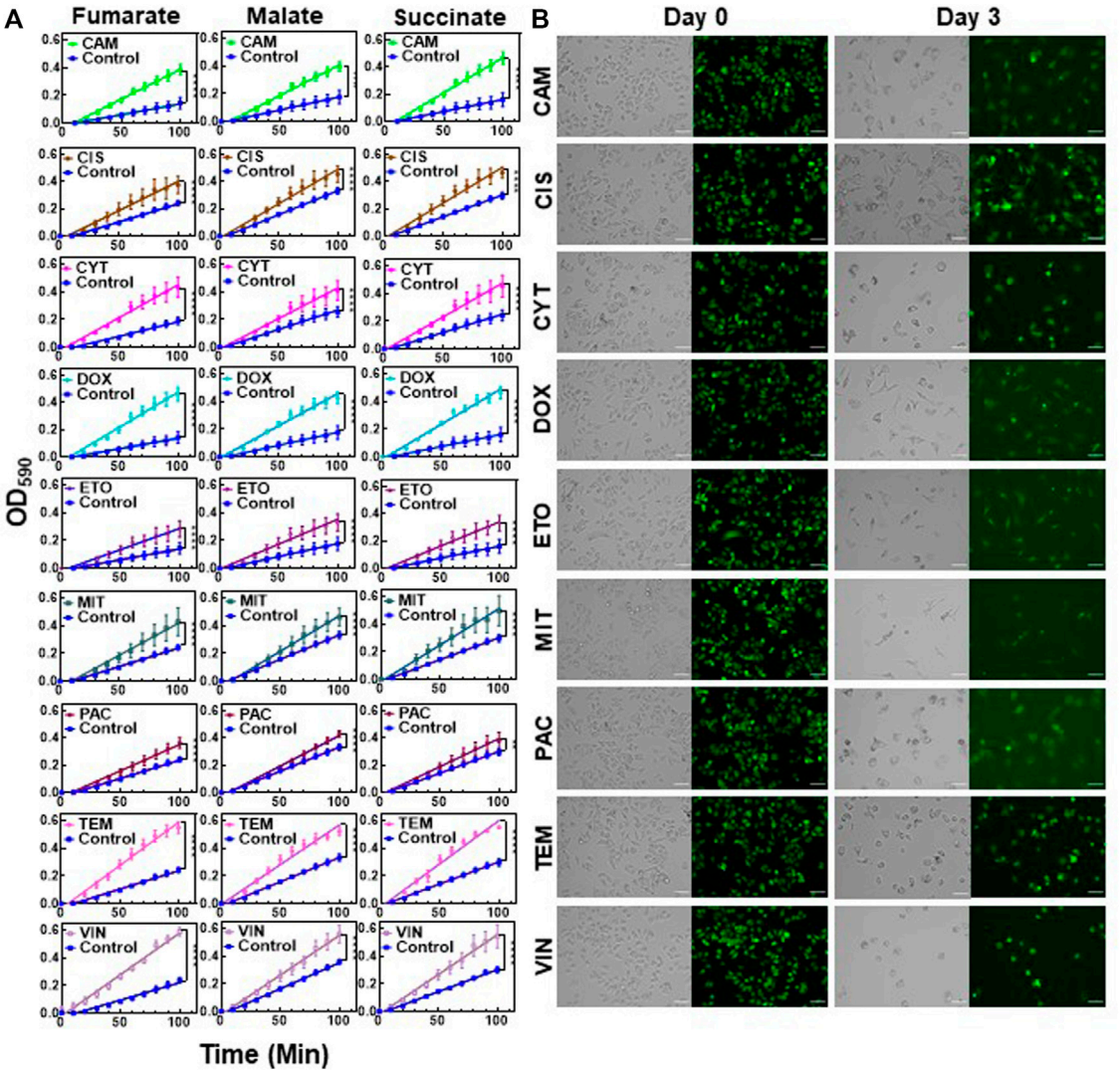

FIGURE 4 | Chemotherapeutic treatments induced slow growth and enhanced Krebs cycle activity: **(A)** Melanoma A375 cells were treated with the indicated chemotherapeutic agents for 3 days. After treatments, the cells were transferred to fresh medium and cultured for 24. h. Then, the cells were collected for modified MitoPlate assays to measure the consumption rates of Krebs cycle substrates. The concentrations of chemotherapeutic agents were 10xIC_{50}, except TEM, whose concentration was 5xIC_{50} (**Supplementary Table S2**). Linear regression analysis was performed using F statistics (****$p < 0.0001$). $N = 4$. **(B)** Melanoma cells stained with CFSE were treated with the indicated agents for 3 days as described above. Prior to treatment (day 0) and after treatment (day 3), the green fluorescence of the cells was monitored by florescence microscopy. Scale bar: 100 μm.

adjuvant (**Figures 5A,B**), although a number of well-known ETC inhibitors, including gossypol, valinomycin, and celastrol, were also found to be effective at higher concentrations (**Supplementary Figure S11**). TFZ falls under the class of antipsychotic drugs known as phenothiazines, which have been shown to enhance the cytotoxic effects of chemotherapeutic agents (Motohashi et al., 2006). These drugs have also been shown to inhibit tumor progression by altering the expression levels of proteins related to cell cycle and apoptosis such as CCNE1, CDK4 and BCL-2, and by inhibiting drug efflux pumps (Spengler et al., 2016; Qian et al., 2019). To determine whether inhibition of persistence is a more general characteristic of phenothiazines, we tested two additional FDA-approved phenothiazine drugs, thioridazine (TDZ) and fluphenazine (FPZ), which were not in our drug screen. Notably, TDZ was recently demonstrated to impair melanoma tumor progression in an animal model (Shen et al., 2020). Although all three phenothiazine inhibitors reduced the cell survival fractions across a wide range of concentrations when tested with GEM (**Figures 5F–H**), these inhibitors (at concentrations greater than 10 μM) could also kill the cancer cells in the absence of GEM (**Figures 5C–E**). TFZ was also found to be effective in the presence of most of the chemotherapeutics at the indicated concentrations (**Figure 5I**). TEM, which is used most often for melanoma patients, has become very effective in the presence of TFZ, as the level of survived cells in cotreatment cultures is

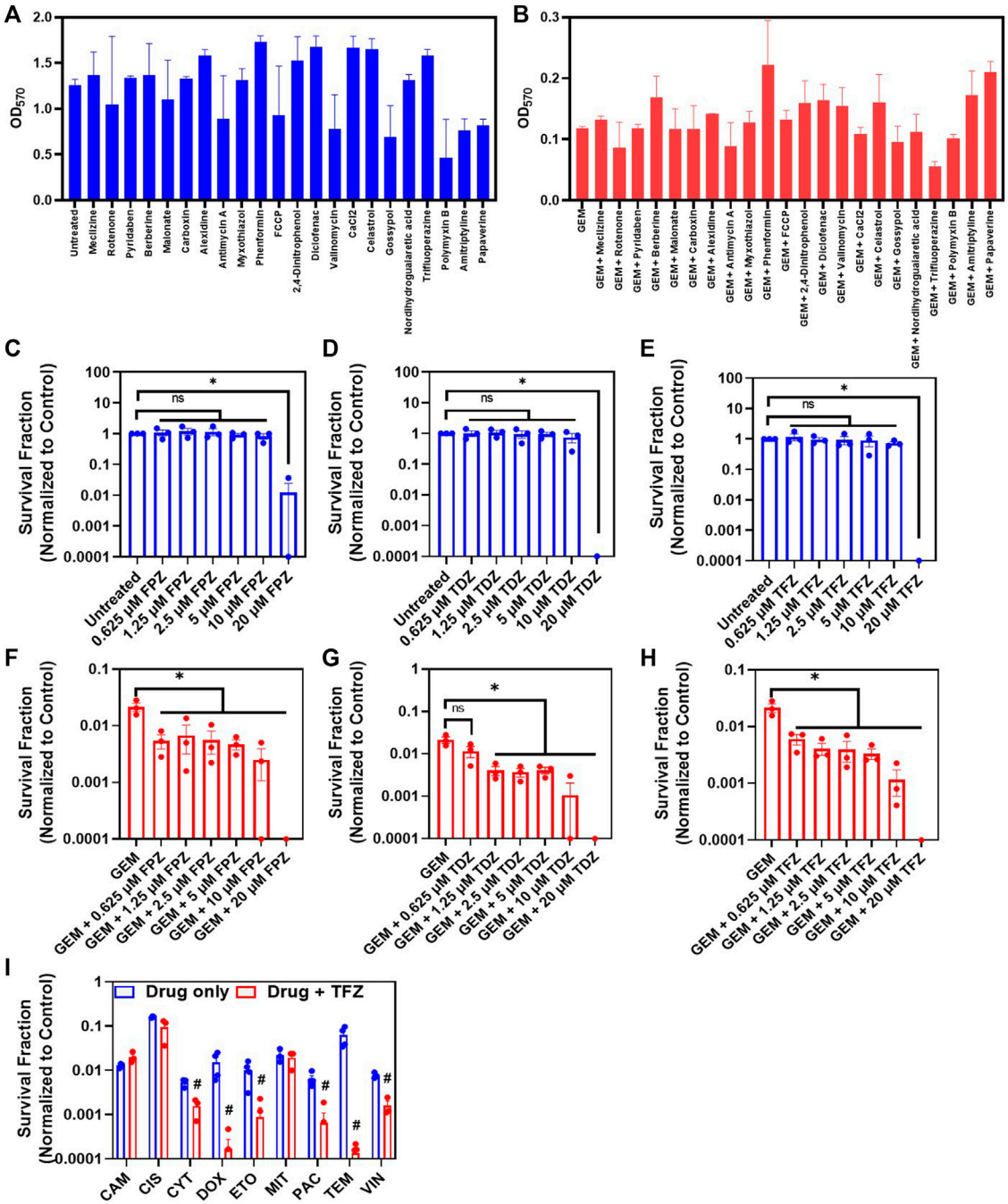

FIGURE 5 | Cotreatment with ETC inhibitors reduces persister survival: **(A)** Melanoma A375 cells incubated in fresh growth medium in a 96-well plate for 24 h were treated with indicated ETC inhibitors (blue) or **(B)** cotreated with GEM (10x MIC) and ETC inhibitors (red) for 3 days. After the treatment, the media in the wells were replaced with fresh, drug-free media. After 24 h of incubation, the MTT assay was conducted to assess cell viability by measuring the absorbance (OD_{570}) of all tested combinations with a plate reader. $N = 2$. **(C–E)** Melanoma cells were treated with phenothiazine drugs (TFZ, TDZ and FPZ) or **(F–H)** co-treated with GEM (10xMIC) and phenothiazines at the indicated concentrations for 3 days. After the treatments, the cells were resuspended in fresh drug-free medium and incubated for 24 h. Then, the cell viability was assessed by trypan blue staining using an automated cell counter. * represents a significant difference between the control and treatment groups (*t*-test, $p < 0.05$). **(I)** Melanoma cells were treated with the indicated chemotherapeutic agents and/or TFZ (10 µM) for 3 days. The concentrations of chemotherapeutic agents were $10xIC_{50}$, except TEM, whose concentration was $5xIC_{50}$ (**Supplementary Table S2**). After the treatments, the cells were collected and incubated in fresh, drug-free medium for 24 h, and then, the cell viability was assessed with STYO60 (red)/SYTOX (green) dyes using a flow cytometer, as the number of surviving cells in some conditions was under the limit of detection for the automated cell counter. # represents a significant difference between the cotreatment (drug + FPZ) and drug-only groups (*t*-test, $p < 0.05$).

around the limit of detection (**Figure 5I**). Although we did not test a wide range of drug concentrations and analyze the synergetic interactions between the drugs in these cotreatments, our results suggest that metabolic inhibitors can potentially boost the effectiveness of the existing chemotherapeutic drugs.

Chemotherapeutic-Induced Metabolic Alteration Is Also Observed in a Metastatic Cell Line (RPMI-7951)

Finally, we used a metastatic melanoma cell line (RPMI-7951) to assess if the observed metabolic alteration is a global response of melanoma cells to chemotherapeutic treatments. RPMI-7951 cells were treated with GEM ($10xIC_{50}$), TEM ($5xIC_{50}$) or left untreated for 3 days, and mitoplate assays were performed following the methods described above. Similar to A375 cells, RPMI-7951 cells treated with chemotherapeutics have significantly increased consumption rates of Krebs-cycle substrates (fumarate, malate and succinate) when compared to untreated control groups (**Supplementary Figures S12A–F**). Furthermore, we co-treated RPMI-7951 cells with TEM and an ETC inhibitor (TFZ) to test the impact of ETC inhibition on RPMI-7951 persistence. We chose TEM for the co-treatment study as it is one of the preferred chemotherapeutic agents for metastasized melanoma treatments (American Cancer Society, 2001). As expected, our data shows that co-treated cultures have reduced persister survival compared to the cultures treated with TEM only (**Supplementary Figures S12G,H**). This observation further shows that targeting the metabolism of drug-tolerant cells can be an effective therapeutic strategy for melanoma cancers.

DISCUSSION

Conventional chemotherapeutic agents target fast-growing cells such as tumor cells. Because of their slow or no-growth state, persister cell tolerance to treatment has been attributed to cell dormancy (Hangauer et al., 2017). *Cancer* cell dormancy can be induced by various mechanisms, such as the activation of signaling pathways for autophagy, reactive oxygen species production, and DNA damage repair, that are generally triggered by extracellular stress (e.g., nutrient depletion, hypoxia, overpopulation, therapeutics) (Recasens and Munoz, 2019; Vallette et al., 2019). Cell dormancy is regulated by many external and internal factors via a highly integrated signaling network and is one of the most common phenotypic states observed in many drug-tolerant cell types. Due to their phenotypic plasticity, melanoma cells may acquire stem cell like characteristics in response to treatments, which may contribute to melanoma cell heterogeneity and drug tolerance. Although persister cells in previous studies were shown to have increased stem cell biomarkers (Raha et al., 2014; Hangauer et al., 2017), we did not observe a drastic change in the expression levels of known stem cell biomarkers in GEM persisters. Our results also indicate that chemotherapeutics may facilitate a transient dormancy, which may lead to the downregulation of anabolic pathways (due to the observed growth arrest), thus diverting glycolytic intermediates to the Krebs cycle, the most efficient energy-producing pathway. This also explains why the abundance of glycolytic metabolites was not altered in persister cells despite the significant alterations in the abundance of Krebs cycle metabolites.

In this study, we first conducted untargeted metabolomics analysis to identify the metabolic pathways that were significantly altered in GEM-treated persister cells compared to control cells. These pathways included the lipid metabolism, BCAA metabolism, one-carbon metabolism, and the Krebs cycle and the PPP. From the lipid superpathways, the levels of phosphatidylcholines, sphingosines, ceramides and lysophospholipids were primarily upregulated in GEM-treated cells. The accumulation of PC due to overexpression of lysophosphatidylcholine acyltransferase 2 (LPCAT2) can induce drug tolerance in cancer cells, as reported by Cotte et al. (2018). The study revealed that LPCAT2 increases the resistance of cancer cells to immunogenic cell death and mediates chemoresistance by promoting the antiapoptotic response to endoplasmic reticulum stressors (Cotte et al., 2018). Ceramides have been reported to have dual functions in drug resistance. They can induce either chemosensitivity or chemoresistance depending on the structure and length of their fatty acyl chains (Brachtendorf et al., 2019).

BCAA metabolism, which involves essential amino acids, such as valine, leucine and isoleucine, has been studied extensively in cancer cells (Ananieva and Wilkinson, 2018). It is closely linked to the Krebs cycle, as alpha-ketoglutarate is needed to initiate the degradation of valine, isoleucine and leucine (Ananieva and Wilkinson, 2018). Enzymes that catalyze the first step of BCAA degradation, branched-chain aminotransferase 1 (BCAT1) and branched-chain aminotransferase 2 (BCAT2), are commonly upregulated in cancer cells. BCAT1 in particular is associated with cancer cell growth and has been proposed as a prognostic cell marker (Zheng et al., 2016; Ananieva and Wilkinson, 2018). In addition, many studies have explored BCAT1 as a potential target for cancer therapeutics, as it is also linked to cell proliferation via m-Torc1 activity (Zhang and Han, 2017). BCAA metabolism has been shown to alter gene expression in cancer cells by altering the epigenome. Epigenetic changes can affect several cellular processes that can induce drug tolerance in cancer cells. A recent study by Wang *et al.* showed that H3K9 demethylation-mediated epigenetic upregulation of BCAT1 can promote tyrosine kinase inhibitor (TKI) tolerance in epidermal growth factor receptor (EGFR)-mutant lung cancer cells (Wang Y. et al., 2019).

The upstream metabolites of the Krebs cycle are needed for the initiation of PPP metabolism. Along with one-carbon metabolism, the PPP regulates NADPH production in cancer cells (Patra and Hay, 2014). Additionally, it has been hypothesized that slow-growing/drug tolerant cells have an increased rate of PPP metabolism compared to the bulk cancer cell population (Lemons et al., 2010). Debeb *et al.* showed that PPP metabolism is upregulated in histone deacetylase inhibitor-induced cancer stem cells and is

regulated by an increase in the level of glucose-6-phosphate dehydrogenase (G6PD), a rate-limiting enzyme in PPP metabolism (Debeb et al., 2016).

DNA repair proteins (e.g., DNA double-strand-break repair proteins) have a major role in metabolic reprogramming of persister cells and mediating their responses to chemo- and radiotherapy (Minchom et al., 2018; Jensena and Rothenberg, 2020). The study conducted by Cosentino et al., 2011, showed that ATM, a key DNA damage protein, regulates PPP via induction of G6PD to promote NADPH and nucleotide production needed for the DNA damage repair (Cosentino et al., 2011). Phosphorylated ATM also enhances mitochondrial respiration and oxidative phosphorylation by increasing the expression of cytochrome c oxidase 2 and glutaminase (Matoba et al., 2006; Suzuki et al., 2010; Wanka et al., 2012). These metabolic alterations, particularly in mitochondria, could enhance the toxicity of chemotherapeutic agents.

Given that MS does not directly measure intracellular reaction rates, subsequent assays are necessary to link the abundance of metabolites to their turnover rates. Our metabolomics data show that the majority of Krebs cycle metabolites were significantly downregulated in GEM-treated cells due to their increased consumption rates, and these findings were verified by MitoPlate assays. It is known that cancer cells prefer aerobic glycolysis; however, as persisters are slow-growing cells, they might not depend on aerobic glycolysis as extensively. The increased mitochondrial metabolism of drug-tolerant cells has been reported across multiple tumor cell lines and in response to a variety of therapeutic challenges (Lee et al., 2017; Echeverria et al., 2019; Shen et al., 2020), supporting our hypothesis of a conserved, transient metabolic phenomenon mediated by chemotherapeutic treatments. Given that increased mitochondrial metabolism is a potentially conserved characteristic of melanoma persistence, ETC inhibitors can be used as adjuvants for persister therapeutics. Although not all ETC inhibitors can be potent and cytotoxic, our findings show that TFZ was highly effective against TEM-tolerant cells. As TEM is a preferred chemotherapeutic agent for the treatment of metastasized melanoma cancers, a co-treatment regime including TEM and an ETC inhibitor can have a potential clinical application. These findings further highlight the significance of understanding and targeting the key metabolic changes in drug-tolerant persister cells.

It is well established that suppression or lack of apoptosis is one of the major factors that increases chemo-resistance (Wilson et al., 2009; Wlodkowic et al., 2009). There are several studies claiming that alterations in certain Bcl-2 family members (e.g., Bcl-2 and Bcl-xL expression level) contribute to multidrug resistance (Schmitt and Lowe, 2001; Johnstone et al., 2002). Persister cells can escape apoptosis and drug cytotoxicity via transient metabolic alterations. However, how these alterations affect apoptotic pathways and consequently cancer persistence remains to be characterized. Finally, we would like to point out that our study has been conducted *in vitro* in a controlled environment; therefore, *in vivo* factors such as cell-cell interactions, micro-environment in the host, treatment regimens and drug clearance may impact persister cell metabolism. Our future goal is to characterize the metabolic state of persister cells in clinically relevant samples or environments, such as patient-derived tissues and animal models.

In this study, we aimed to evaluate the role of metabolism in melanoma persister cells and the utility of targeting persister cell metabolism as a therapeutic strategy. Melanoma which is the most fatal form of skin cancer is thought to be a chemotherapy-resistant cancer type, and this resistance is potentially facilitated by slow-growing persister cells. Our analysis shows that chemotherapeutic agents can facilitate persister cell formation in melanoma cells and alter cellular metabolism by upregulating the utilization rates of Krebs cycle metabolites. The observed metabolic alteration seems to be independent of drug concentration and treatment time, and can be mediated by a wide range of chemotherapeutic agents.

DATA AVAILABILITY STATEMENT

The original contributions presented in the study are included in the article/**Supplementary Material**. Further inquiries can be directed to the corresponding author.

AUTHOR CONTRIBUTIONS

PK, VA and MO designed the study and interpreted the data. PK and VA performed the cell experiments. JM analyzed the transcriptomics data analysis. MO supervised the research and wrote the manuscript with PK, VA and JM.

FUNDING

The research was supported by the University of Houston startup grant.

ACKNOWLEDGMENTS

We thank the members of the Orman Lab research group for their valuable contributions to this project. We also thank Barry Bochner and Brendan Lewis from Biolog, Inc., for providing us valuable insights and suggestions about our study.

SUPPLEMENTARY MATERIAL

The Supplementary Material for this article can be found online at: https://www.frontiersin.org/articles/10.3389/fmolb.2021.780192/full#supplementary-material

REFERENCES

American Cancer Society (2001). American Cancer Society. *J. Investig. Med.* 49, 462. doi:10.2310/6650.2001.33798

Ananieva, E. A., and Wilkinson, A. C. (2018). Branched-chain Amino Acid Metabolism in Cancer. *Curr. Opin. Clin. Nutr. Metab. Care* 21, 64–70. doi:10.1097/MCO.0000000000000430

Arinbasarova, A. Y., Medentsev, A. G., and Krupyanko, V. I. (2012). Gossypol Inhibits Electron Transport and Stimulates ROS Generation in Yarrowia Lipolytica Mitochondria. *Open Biochem. J.* 6, 11–15. doi:10.2174/1874091x01206010011

Brachtendorf, S., El-Hindi, K., and Grösch, S. (2019). Ceramide Synthases in Cancer Therapy and Chemoresistance. *Prog. Lipid Res.* 74, 160–185. doi:10.1016/j.plipres.2019.04.002

Chen, G., Zhang, X., Zhao, M., Wang, Y., Cheng, X., Wang, D., et al. (2011). Celastrol Targets Mitochondrial Respiratory Chain Complex I to Induce Reactive Oxygen Species-dependent Cytotoxicity in Tumor Cells. *BMC Cancer* 11, 170. doi:10.1186/1471-2407-11-170

Cosentino, C., Grieco, D., and Costanzo, V. (2011). ATM Activates the Pentose Phosphate Pathway Promoting Anti-oxidant Defence and DNA Repair. *EMBO J.* 30, 546–555. doi:10.1038/emboj.2010.330

Cotte, A. K., Aires, V., Fredon, M., Limagne, E., Derangère, V., Thibaudin, M., et al. (2018). Lysophosphatidylcholine Acyltransferase 2-mediated Lipid Droplet Production Supports Colorectal Cancer Chemoresistance. *Nat. Commun.* 9, 1–16. doi:10.1038/s41467-017-02732-5

Davies, H., Bignell, G. R., Cox, C., Stephens, P., Edkins, S., Clegg, S., et al. (2002). Mutations of the BRAF Gene in Human Cancer. *Nature* 417, 949–954. doi:10.1038/nature00766

Debeb, B. G., Lacerda, L., Larson, R., Wolfe, A. R., Krishnamurthy, S., Reuben, J. M., et al. (2016). Histone Deacetylase Inhibitor-Induced Cancer Stem Cells Exhibit High Pentose Phosphate Pathway Metabolism. *Oncotarget* 7, 28329–28339. doi:10.18632/oncotarget.8631

Echeverria, G. V., Ge, Z., Seth, S., Zhang, X., Jeter-Jones, S., Zhou, X., et al. (2019). Resistance to Neoadjuvant Chemotherapy in Triple-Negative Breast Cancer Mediated by a Reversible Drug-Tolerant State. *Sci. Transl. Med.* 11, 936. doi:10.1126/scitranslmed.aav0936

Evans, A. M., DeHaven, C. D., Barrett, T., Mitchell, M., and Milgram, E. (2009). Integrated, Nontargeted Ultrahigh Performance Liquid Chromatography/Electrospray Ionization Tandem Mass Spectrometry Platform for the Identification and Relative Quantification of the Small-Molecule Complement of Biological Systems. *Anal. Chem.* 81, 6656–6667. doi:10.1021/ac901536h

Hanahan, D., and Weinberg, R. A. (2011). Hallmarks of Cancer: The Next Generation. *Cell* 144, 646–674. doi:10.1016/j.cell.2011.02.013

Hangauer, M. J., Viswanathan, V. S., Ryan, M. J., Bole, D., Eaton, J. K., Matov, A., et al. (2017). Drug-tolerant Persister Cancer Cells Are Vulnerable to GPX4 Inhibition. *Nature* 551, 247–250. doi:10.1038/nature24297

He, G., Siddik, Z. H., Huang, Z., Wang, R., Koomen, J., Kobayashi, R., et al. (2005). Induction of P21 by P53 Following DNA Damage Inhibits Both Cdk4 and Cdk2 Activities. *Oncogene* 24, 2929–2943. doi:10.1038/sj.onc.1208474

Held, M. A., Curley, D. P., Dankort, D., McMahon, M., Muthusamy, V., and Bosenberg, M. W. (2010). Characterization of Melanoma Cells Capable of Propagating Tumors from a Single Cell. *Cancer Research* 70 (1), 388–397. doi:10.1158/0008-5472

Huang, L.-s., Cobessi, D., Tung, E. Y., and Berry, E. A. (2005). Binding of the Respiratory Chain Inhibitor Antimycin to the Mitochondrial Bc1 Complex: A New crystal Structure Reveals an Altered Intramolecular Hydrogen-Bonding Pattern. *J. Mol. Biol.* 351, 573–597. doi:10.1016/j.jmb.2005.05.053

Iorio, F., Knijnenburg, T. A., Vis, D. J., Bignell, G. R., Menden, M. P., Schubert, M., et al. (2016). A Landscape of Pharmacogenomic Interactions in Cancer. *Cell* 166, 740–754. doi:10.1016/j.cell.2016.06.017

Islam, S. R., and Manna, S. K. (2019). "Lipidomic Analysis of Cancer Cell and Tumor Tissues," in *Methods in Molecular Biology* (New York, NY: Humana Press), 175–204. doi:10.1007/978-1-4939-9027-6_11

Jemal, A., Siegel, R., and Miller, K. D. (2018). Home | American Cancer Society - Cancer Facts & Statistics. *Cancer Stat. Cent.* Available at: https://cancerstatisticscenter.cancer.org/?_ga=2.119354625.981350640.1612278063-1675888105.1612278063#!/(Accessed February 2, 2021).

Jensen, R. B., and Rothenberg, E. (2020). Preserving Genome Integrity in Human Cells via DNA Double-Strand Break Repair. *MBoC* 31, 859–865. doi:10.1091/MBC.E18-10-0668

Johnstone, R. W., Ruefli, A. A., and Lowe, S. W. (2002). Apoptosis. *Cell* 108, 153–164. doi:10.1016/S0092-8674(02)00625-6

Keenan, A. B., Jenkins, S. L., Jagodnik, K. M., Koplev, S., He, E., Torre, D., et al. (2018). The Library of Integrated Network-Based Cellular Signatures NIH Program: System-Level Cataloging of Human Cells Response to Perturbations. *Cell Syst* 6, 13–24. doi:10.1016/j.cels.2017.11.001

Keener, A. B. (2016). Shapeshifters in Cancer: How Some Tumor Cells Change Phenotype to Evade Therapy. *Nat. Med.* 22, 1194–1196. doi:10.1038/nm1116-1194

Koolen, P. G. L., Matos, T. R., Ibrahim, A. M. S., Sun, J., Lee, B. T., Frankenthaler, R. A., et al. (2017). Recurrence Rates over 20 Years in the Treatment of Malignant Melanoma. *Plast. Reconstr. Surg. - Glob. Open* 5, e1378. doi:10.1097/GOX.0000000000001378

Kopecka, J., Trouillas, P., Gašparović, A. Č., Gazzano, E., Assaraf, Y. G., and Riganti, C. (2020). Phospholipids and Cholesterol: Inducers of Cancer Multidrug Resistance and Therapeutic Targets. *Drug Resist. Updates* 49, 100670. doi:10.1016/j.drup.2019.100670

Lee, K.-m., Giltnane, J. M., Balko, J. M., Schwarz, L. J., Guerrero-Zotano, A. L., Hutchinson, K. E., et al. (2017). MYC and MCL1 Cooperatively Promote Chemotherapy-Resistant Breast Cancer Stem Cells via Regulation of Mitochondrial Oxidative Phosphorylation. *Cel Metab.* 26, 633–647. e7. doi:10.1016/j.cmet.2017.09.009

Lemons, J. M. S., Feng, X.-J., Bennett, B. D., Legesse-Miller, A., Johnson, E. L., Raitman, I., et al. (2010). Quiescent Fibroblasts Exhibit High Metabolic Activity. *Plos Biol.* 8, e1000514. doi:10.1371/journal.pbio.1000514

Li, N., Ragheb, K., Lawler, G., Sturgis, J., Rajwa, B., Melendez, J. A., et al. (2003). Mitochondrial Complex I Inhibitor Rotenone Induces Apoptosis through Enhancing Mitochondrial Reactive Oxygen Species Production. *J. Biol. Chem.* 278, 8516–8525. doi:10.1074/jbc.M210432200

Liberti, M. V., and Locasale, J. W. (2016). The Warburg Effect: How Does it Benefit Cancer Cells? *Trends Biochem. Sci.* 41, 211–218. doi:10.1016/j.tibs.2015.12.001

Liu, J., Zhang, C., Hu, W., and Feng, Z. (2019). Tumor Suppressor P53 and Metabolism. *J. Mol. Cel Biol.* 11, 284–292. doi:10.1093/jmcb/mjy070

Lofrumento, D. D., La Piana, G., Abbrescia, D. I., Palmitessa, V., La Pesa, V., and Marzulli, D. (2011). Valinomycin Induced Energy-dependent Mitochondrial Swelling, Cytochrome c Release, Cytosolic NADH/cytochrome c Oxidation and Apoptosis. *Apoptosis* 16 (10), 1004–1013. doi:10.1007/s10495-011-0628-7

Louis, K. S., and Siegel, A. C. (2011). Cell Viability Analysis Using Trypan Blue: Manual and Automated Methods. *Methods Mol. Biol.* 740, 7–12. doi:10.1007/978-1-61779-108-6_2

Luo, Y., Dallaglio, K., Chen, Y., Robinson, W. A., Robinson, S. E., McCarter, M. D., et al. (2012). ALDH1A Isozymes Are Markers of Human Melanoma Stem Cells and Potential Therapeutic Targets. *Stem Cells* 30, 2100–2113. doi:10.1002/stem.1193

Lyons, A. B., and Parish, C. R. (1994). Determination of Lymphocyte Division by Flow Cytometry. *J. Immunological Methods* 171, 131–137. doi:10.1016/0022-1759(94)90236-4

Matoba, S., Kang, J.-G., Patino, W. D., Wragg, A., Boehm, M., Gavrilova, O., et al. (2006). p53 Regulates Mitochondrial Respiration. *Science* 312, 1650–1653. doi:10.1126/science.1126863

Miller, K. D., Nogueira, L., Mariotto, A. B., Rowland, J. H., Yabroff, K. R., Alfano, C. M., et al. (2019). Cancer Treatment and Survivorship Statistics, 2019. *Cancer J. Clin.* 69, 363–385. doi:10.3322/caac.21565

Minchom, A., Aversa, C., and Lopez, J. (2018). Dancing with the DNA Damage Response: Next-Generation Anti-cancer Therapeutic Strategies. *Ther. Adv. Med. Oncol.* 10, 175883591878665. doi:10.1177/1758835918786658

Motohashi, N., Kawase, M., Satoh, K., and Sakagami, H. (2006). Cytotoxic Potential of Phenothiazines. *Cdt* 7, 1055–1066. doi:10.2174/138945006778226624

Newman, A. C., and Maddocks, O. D. K. (2017). One-carbon Metabolism in Cancer. *Br. J. Cancer* 116, 1499–1504. doi:10.1038/bjc.2017.118

Niepel, M., Hafner, M., Mills, C. E., Subramanian, K., Williams, E. H., Chung, M., et al. (2019). A Multi-center Study on the Reproducibility of Drug-Response

Assays in Mammalian Cell Lines. *Cel Syst.* 9, 35–48. e5. doi:10.1016/j.cels.2019.06.005

Noble, S., and Goa, K. L. (1997). Gemcitabine. *Drugs* 54, 447–472. doi:10.2165/00003495-199754030-00009

Patra, K. C., and Hay, N. (2014). The Pentose Phosphate Pathway and Cancer. *Trends Biochem. Sci.* 39, 347–354. doi:10.1016/j.tibs.2014.06.005

Paulis, Y. W. J., Huijbers, E. J. M., van der Schaft, D. W. J., Soetekouw, P. M. M. B., Pauwels, P., Tjan-Heijnen, V. C. G., et al. (2015). CD44 Enhances Tumor Aggressiveness by Promoting Tumor Cell Plasticity. *Oncotarget* 6, 19634–19646. doi:10.18632/oncotarget.3839

Ponnusamy, S., Meyers-Needham, M., Senkal, C. E., Saddoughi, S. A., Sentelle, D., Selvam, S. P., et al. (2010). Sphingolipids and Cancer: Ceramide and Sphingosine-1-Phosphate in the Regulation of Cell Death and Drug Resistance. *Future Oncol.* 6, 1603–1624. doi:10.2217/fon.10.116

Qian, K., Sun, L., Zhou, G., Ge, H., Meng, Y., Li, J., et al. (2019). Trifluoperazine as an Alternative Strategy for the Inhibition of Tumor Growth of Colorectal Cancer. *J. Cell. Biochem.* 120, 15756–15765. doi:10.1002/jcb.28845

Raha, D., Wilson, T. R., Peng, J., Peterson, D., Yue, P., Evangelista, M., et al. (2014). The Cancer Stem Cell Marker Aldehyde Dehydrogenase Is Required to Maintain a Drug-Tolerant Tumor Cell Subpopulation. *Cancer Res.* 74, 3579–3590. doi:10.1158/0008-5472.CAN-13-3456

Rambow, F., Marine, J.-C., and Goding, C. R. (2019). Melanoma Plasticity and Phenotypic Diversity: Therapeutic Barriers and Opportunities. *Genes Dev.* 33, 1295–1318. doi:10.1101/gad.329771.119

Ramirez, M., Rajaram, S., Steininger, R. J., Osipchuk, D., Roth, M. A., Morinishi, L. S., et al. (2016). Diverse Drug-Resistance Mechanisms Can Emerge from Drug-Tolerant Cancer Persister Cells. *Nat. Commun.* 7. doi:10.1038/ncomms10690

Recasens, A., and Munoz, L. (2019). Targeting Cancer Cell Dormancy. *Trends Pharmacol. Sci.* 40, 128–141. doi:10.1016/j.tips.2018.12.004

Restivo, G., Diener, J., Cheng, P. F., Kiowski, G., Bonalli, M., Biedermann, T., et al. (2017). The Low Affinity Neurotrophin Receptor CD271 Regulates Phenotype Switching in Melanoma. *Nat. Commun.* 8 (1), 1–16. doi:10.1038/s41467-017-01573-6

Reinhardt, H. C., Aslanian, A. S., Lees, J. A., and Yaffe, M. B. (2007). p53-Deficient Cells Rely on ATM- and ATR-Mediated Checkpoint Signaling through the p38MAPK/MK2 Pathway for Survival after DNA Damage. *Cancer Cell* 11, 175–189. doi:10.1016/j.ccr.2006.11.024

Riss, T. L., Moravec, R. A., Niles, A. L., Duellman, S., Benink, H. A., Worzella, T. J., et al. (2004). *Cell Viability Assays*. Bethesda, MD: Eli Lilly & Company and the National Center for Advancing Translational Sciences. Available at: http://www.ncbi.nlm.nih.gov/pubmed/23805433 (Accessed February 4, 2021).

Roesch, A., Vultur, A., Bogeski, I., Wang, H., Zimmermann, K. M., Speicher, D., et al. (2013). Overcoming Intrinsic Multidrug Resistance in Melanoma by Blocking the Mitochondrial Respiratory Chain of Slow-Cycling JARID1Bhigh Cells. *Cancer Cell* 23, 811–825. doi:10.1016/j.ccr.2013.05.003

Schmitt, C. A., and Lowe, S. W. (2001). Bcl-2 Mediates Chemoresistance in Matched Pairs of Primary Eμ-Myc Lymphomas *In Vivo*. *Blood Cell Mol. Dis.* 27, 206–216. doi:10.1006/bcmd.2000.0372

Sciacovelli, M., Gaude, E., Hilvo, M., and Frezza, C. (2014). "The Metabolic Alterations of Cancer Cells," in *Methods in Enzymology* (Academic Press), 1–23. doi:10.1016/B978-0-12-416618-9.00001-7

SEER Cancer Statistics (2007). Review 1975-2007 - Previous Version - SEER Cancer Statistics. Available at: https://seer.cancer.gov/archive/csr/1975_2007/ (Accessed February 2, 2021).

Sharma, S. V., Lee, D. Y., Li, B., Quinlan, M. P., Takahashi, F., Maheswaran, S., et al. (2010). A Chromatin-Mediated Reversible Drug-Tolerant State in Cancer Cell Subpopulations. *Cell* 141, 69–80. doi:10.1016/j.cell.2010.02.027

Shen, S., Faouzi, S., Bastide, A., Martineau, S., Malka-Mahieu, H., Fu, Y., et al. (2019). An Epitranscriptomic Mechanism Underlies Selective mRNA Translation Remodelling in Melanoma Persister Cells. *Nat. Commun.* 10. doi:10.1038/s41467-019-13360-6

Shen, S., Faouzi, S., Souquere, S., Roy, S., Routier, E., Libenciuc, C., et al. (2020). Melanoma Persister Cells Are Tolerant to BRAF/MEK Inhibitors via ACOX1-Mediated Fatty Acid Oxidation. *Cel Rep.* 33, 108421. doi:10.1016/j.celrep.2020.108421

Shimomura, Y., and Kitaura, Y. (2018). Physiological and Pathological Roles of Branched-Chain Amino Acids in the Regulation of Protein and Energy Metabolism and Neurological Functions. *Pharmacol. Res.* 133, 215–217. doi:10.1016/j.phrs.2018.05.014

Spengler, G., Csonka, Á., Molnár, J., and Amaral, L. (2016). The Anticancer Activity of the Old Neuroleptic Phenothiazine-type Drug Thioridazine. *Ar* 36, 5701–5706. doi:10.21873/anticanres.11153

Stincone, A., Prigione, A., Cramer, T., Wamelink, M. M. C., Campbell, K., Cheung, E., et al. (2015). The Return of Metabolism: Biochemistry and Physiology of the Pentose Phosphate Pathway. *Biol. Rev.* 90, 927–963. doi:10.1111/brv.12140

Suzuki, S., Tanaka, T., Poyurovsky, M. V., Nagano, H., Mayama, T., Ohkubo, S., et al. (2010). Phosphate-activated Glutaminase (GLS2), a P53-Inducible Regulator of Glutamine Metabolism and Reactive Oxygen Species. *Proc. Natl. Acad. Sci.* 107, 7461–7466. doi:10.1073/pnas.1002459107

Vallette, F. M., Olivier, C., Lézot, F., Oliver, L., Cochonneau, D., Lalier, L., et al. (2019). Dormant, Quiescent, Tolerant and Persister Cells: Four Synonyms for the Same Target in Cancer. *Biochem. Pharmacol.* 162, 169–176. doi:10.1016/j.bcp.2018.11.004

Van Engeland, M., Nieland, L. J. W., Ramaekers, F. C. S., Schutte, B., and Reutelingsperger, C. P. M. (1998). Annexin V-Affinity Assay: A Review on an Apoptosis Detection System Based on Phosphatidylserine Exposure. *Cytometry* 31, 1–9. doi:10.1002/(sici)1097-0320(19980101)31:1<1::aid-cyto1>3.0.co;2-r

Viale, A., Pettazzoni, P., Lyssiotis, C. A., Ying, H., Sánchez, N., Marchesini, M., et al. (2014). Oncogene Ablation-Resistant Pancreatic Cancer Cells Depend on Mitochondrial Function. *Nature* 514, 628–632. doi:10.1038/nature13611

Vincelette, N. D., and Yun, S. (2014). Assessing the Mechanism of Cytarabine-Induced Killing in Acute Leukemia. *Blood* 124, 5210. doi:10.1182/blood.v124.21.5210.5210

Wang, L., Yang, Q., Peng, S., and Liu, X. (2019a). The Combination of the Glycolysis Inhibitor 2-DG and Sorafenib Can Be Effective against Sorafenib-Tolerant Persister Cancer Cells. *Ott* 12, 5359–5373. doi:10.2147/OTT.S212465

Wang, Y., Zhang, J., Ren, S., Sun, D., Huang, H.-Y., Wang, H., et al. (2019b). Branched-Chain Amino Acid Metabolic Reprogramming Orchestrates Drug Resistance to EGFR Tyrosine Kinase Inhibitors. *Cel Rep.* 28, 512–525. e6. doi:10.1016/j.celrep.2019.06.026

Wanka, C., Brucker, D. P., Bähr, O., Ronellenfitsch, M., Weller, M., Steinbach, J. P., et al. (2012). Synthesis of Cytochrome C Oxidase 2: A P53-dependent Metabolic Regulator that Promotes Respiratory Function and Protects Glioma and colon Cancer Cells from Hypoxia-Induced Cell Death. *Oncogene* 31, 3764–3776. doi:10.1038/onc.2011.530

Warburg, O. (1923). Tests on Surviving Carcinoma Cultures. *Biochem. Z.* 142, 317–333. Available at: https://scholar.google.com/scholar_lookup?title=Tests on surviving carcinoma cultures&publication_year=1923&author=O. Warburg (Accessed February 2, 2021).

Warburg, O. (1925). The Metabolism of Carcinoma Cells. *J. Cancer Res.* 9, 148–163. doi:10.1158/jcr.1925.148

Wilson, T., Johnston, P., and Longley, D. (2009). Anti-Apoptotic Mechanisms of Drug Resistance in Cancer. *Ccdt* 9, 307–319. doi:10.2174/156800909788166547

Wishart, D. S., Knox, C., Guo, A. C., Shrivastava, S., Hassanali, M., Stothard, P., et al. (2006). DrugBank: a Comprehensive Resource for In Silico Drug Discovery and Exploration. *Nucleic Acids Res.* 34, D668–D672. doi:10.1093/nar/gkj067

Wlodkowic, D., Skommer, J., and Darzynkiewicz, Z. (2009). Flow Cytometry-Based Apoptosis Detection. *Methods Mol. Biol.* 559, 19–32. doi:10.1007/978-1-60327-017-5_2

Woods, D., and Turchi, J. J. (2013). Chemotherapy Induced DNA Damage Response. *Cancer Biol. Ther.* 14, 379–389. doi:10.4161/cbt.23761

Yang, W., Soares, J., Greninger, P., Edelman, E. J., Lightfoot, H., Forbes, S., et al. (2013). Genomics of Drug Sensitivity in Cancer (GDSC): A Resource for Therapeutic Biomarker Discovery in Cancer Cells. *Nucleic Acids Res.* 41, D955–D961. doi:10.1093/nar/gks1111

Zhang, L., and Han, J. (2017). Branched-chain Amino Acid Transaminase 1 (BCAT1) Promotes the Growth of Breast Cancer Cells through Improving mTOR-Mediated Mitochondrial Biogenesis and Function. *Biochem. Biophysical Res. Commun.* 486, 224–231. doi:10.1016/j.bbrc.2017.02.101

Zheng, Y.-H., Hu, W.-J., Chen, B.-C., Grahn, T.-H. -M., Zhao, Y.-R., Bao, H.-L., et al. (2016). BCAT1, a Key Prognostic Predictor of Hepatocellular Carcinoma,

Promotes Cell Proliferation and Induces Chemoresistance to Cisplatin. *Liver Int.* 36, 1836–1847. doi:10.1111/liv.13178

Conflict of Interest: The authors declare that the research was conducted in the absence of any commercial or financial relationships that could be construed as a potential conflict of interest.

Publisher's Note: All claims expressed in this article are solely those of the authors and do not necessarily represent those of their affiliated organizations, or those of the publisher, the editors and the reviewers. Any product that may be evaluated in this article, or claim that may be made by its manufacturer, is not guaranteed or endorsed by the publisher.